Mon. Not. R. Astron. Soc. **315**, 543–569 (2000)

Comprehensive analytic formulae for stellar evolution as a function of mass and metallicity

Jarrod R. Hurley,[1★] Onno R. Pols[2★] and Christopher A. Tout[1★]
[1]*Institute of Astronomy, Madingley Road, Cambridge CB3 0HA*
[2]*Instituto de Astrofísica de Canarias, c/Via Láctea s/n, E-38200 La Laguna, Tenerife, Spain*

Accepted 2000 January 27. Received 1999 September 22

ABSTRACT

We present analytic formulae that approximate the evolution of stars for a wide range of mass M and metallicity Z. Stellar luminosity, radius and core mass are given as a function of age, M and Z, for all phases from the zero-age main sequence up to, and including, the remnant stages. For the most part we find continuous formulae accurate to within 5 per cent of detailed models. These formulae are useful for purposes such as population synthesis that require very rapid but accurate evaluation of stellar properties, and in particular for use in combination with N-body codes. We describe a mass-loss prescription that can be used with these formulae, and investigate the resulting stellar remnant distribution.

Key words: methods: analytical – stars: evolution – stars: fundamental parameters – stars: mass-loss – stars: Population II – galaxies: stellar content.

1 INTRODUCTION

The results of detailed stellar evolution calculations are required for applications in many areas of astrophysics. Examples include modelling the chemical evolution of galaxies, determining the ages of star clusters, and simulating the outcomes of stellar collisions. As stellar evolution theory, and our ability to model it, is continually being improved (the treatment of convective overshooting and thermal pulses, for example) there is an ongoing need to update the results of these calculations. For a recent overview of problems in stellar evolution see Noels et al. (1995).

As with all theories, our understanding of stellar evolution must be tested against observations. One way to do this is to attempt to reproduce the findings of large-scale star surveys, such as the Bright Star Catalogue (Hoffleit 1983) and the Hipparcos Catalogue (Perryman et al. 1997), using population synthesis. The Hipparcos Catalogue is an excellent example of how improved observing techniques can initiate a re-evaluation of many aspects of stellar evolution theory (Baglin 1997; de Boer, Tucholke & Schmidt 1997; Van Eck et al. 1998). In order to make population synthesis statistically meaningful, it is necessary to evolve a large sample of stars so as to overcome Poisson noise. If we synthesize n examples of a particular type of star, we have an error of $\pm\sqrt{n}$, which means that for rarer stars often millions of possible progenitors are required to get a sufficently accurate sample. However, detailed evolution codes can take several hours to evolve a model of just one star. Thus it is desirable to generate a large set of detailed models and present them in some convenient form in which it is relatively simple to utilize the results at a later stage.

There are two alternative approaches to the problem of using the output of a series of stellar-evolution runs as data for projects that require them. One approach is to construct tables (necessarily rather large, especially if a range of metallicities and/or overshoot parameter is to be incorporated) and interpolate within these tables. The other is to approximate the data by a number of interpolation formulae as functions of age, mass and metallicity. Both procedures have advantages and disadvantages (Eggleton 1996), so we have worked on both simultaneously. Stellar models have been available in tabular form for many years (Schaller et al. 1992; Charbonnel et al. 1993; Mowlavi et al. 1998). Stellar populations cover a wide range of metallicity, so the ideal is to have a set of models that cover the full range of possible compositions and stellar masses. In a previous paper (Pols et al. 1998) we presented the results of stellar evolution calculations for a wide range of mass and metallicity in tabular form. In the present paper we report on the results of the second approach, construction of a set of single-star evolution (SSE) formulae, thus expanding the work of Eggleton, Fitchett & Tout (1989) along the lines of Tout et al. (1996). It is more difficult in practice to find analytic approximations of a conveniently simple nature for the highly non-uniform movement of a star in the Hertzsprung–Russell diagram (HRD) than it is to interpolate in tables, but the resulting code is very much more compact and adaptable to the requirements of, for example, an N-body code (Aarseth 1996) or variable mass-loss. This is reinforced in the circumstance where one wishes to include binary-star interactions, such as Roche-lobe overflow, common-envelope evolution, and magnetic braking with tidal friction, for example (Tout et al. 1997).

★ E-mail: jhurley@ast.cam.ac.uk (JRH); onno@ll.iac.es (ORP); cat@ast.cam.ac.uk (CAT)

In Section 2 we provide a brief overview of how stars behave as they evolve in time, which introduces some of the terminology that we use and will hopefully facilitate the understanding of this paper. Section 3 describes the detailed models from which the formulae are derived, and justifies the inclusion of enhanced mixing processes. In Section 4 we outline the procedure to be used for generating the SSE package. The evolution formulae are presented in Section 5 for all nuclear burning phases from the main sequence to the asymptotic giant branch. Our formulae are a vast improvement on the work of Eggleton et al. (1989), not only due to the inclusion of metallicity as a free parameter but also because we have taken a great deal of effort to provide a more detailed and accurate treatment of all phases of the evolution. Features such as main-sequence formulae that are continuous over the entire mass range and the modelling of second dredge-up and thermal pulses will be discussed. Section 6 discusses the behaviour of a star as the stellar envelope becomes small in mass and outlines what happens when the nuclear evolution is terminated. We also provide formulae which model the subsequent remnant phases of evolution. In Section 7 we describe a comprehensive mass-loss algorithm which can be used in conjunction with the evolution formulae, as well as a method for modelling stellar rotation. Various uses for the formulae and future improvements are discussed in Section 8, along with details of how to obtain the formulae in convenient subroutine form.

2 STELLAR EVOLUTION OVERVIEW

A fundamental tool in understanding stellar evolution is the Hertzsprung–Russell diagram (HRD), which provides a correlation between the observable stellar properties of luminosity, L, and effective surface temperature, $T_{\rm eff}$. Fig. 1 shows the evolution of a selection of stars in the HRD from the zero-age main sequence (ZAMS), where a star adjusts itself to nuclear burning equilibrium, until the end of their nuclear burning lifetimes. As stars take a relatively short time to reach the ZAMS, all ages are measured from this point. The length of a star's life, its path on the HRD, and its ultimate fate depend critically on its mass.

Stars spend most of their time on or near the main sequence (MS) burning hydrogen to produce helium in their cores. To first order, the behaviour of a star on the MS can be linked to whether it has a radiative or convective core. Stars with $M \lesssim 1.1\,{\rm M}_{\odot}$ have radiative cores, while in higher mass stars a convective core develops as a result of the steep temperature gradient in the interior. During core hydrogen burning on the MS, low-mass stars will move upwards in L and to higher $T_{\rm eff}$ on the HRD, while higher mass stars will also move upwards in L but to a region of lower $T_{\rm eff}$. The MS evolution will end when the star has exhausted its supply of hydrogen in the core. Low-mass stars will continue expanding as they evolve off the MS, but for higher mass stars with convective cores the transition is not so smooth. Owing to mixing in the core there is a sudden depletion of fuel over a large region, which leads to a rapid contraction over the inner region at core-hydrogen exhaustion. This causes the hydrogen-exhausted phase gap, or MS hook, which occurs on a thermal time-scale. The different features of MS evolution are illustrated by comparing the evolution tracks for the 1.0-$\rm M_{\odot}$ and 1.6-$\rm M_{\odot}$ stars in Fig. 1.

The immediate post-MS evolution towards the right in the HRD occurs at nearly constant luminosity and is very rapid. For this reason very few stars are seen in this phase, and this region of the HRD is called the Hertzsprung gap (HG), or the subgiant branch. During this HG phase the radius of the star increases greatly, causing a decrease in $T_{\rm eff}$. For cool envelope temperatures the opacity increases, causing a convective envelope to develop. As the convective envelope grows in extent, the star will reach the giant branch (GB), which is the nearly vertical line corresponding to a fully convective star, also known as the Hayashi track. All stars ascend the GB, with the hydrogen-exhausted core contracting slowly in radius and heating while the hydrogen-burning shell is eating its way outwards in mass and leaving behind helium to add to the growing core. As the stars move up the GB, convection extends over an increasing portion of the star. The convective envelope may even reach into the previously burnt (or processed) regions, so that burning products are mixed to the surface in a process called dredge-up.

Eventually, a point is reached on the GB where the core temperature is high enough for stars to ignite their central helium supply. For massive stars, $M \gtrsim 2.0\,{\rm M}_{\odot}$, this takes place gently. When core helium burning (CHeB) begins, the star descends along the GB until contraction moves the star away from the fully convective region of the HRD and back towards the MS in what is called a blue loop. During CHeB, carbon and oxygen are produced in the core. Eventually, core helium is exhausted and the star moves back to the right in the HRD. The size of the blue loop generally increases with mass, as can be seen by comparing the 4.0-$\rm M_{\odot}$ and 10.0-$\rm M_{\odot}$ tracks in Fig. 1. Lower mass stars have degenerate helium cores on the GB, leading to an abrupt core-helium flash at helium ignition (HeI). The star then moves down to the zero-age horizontal branch (ZAHB) very quickly. The initial position of a star along the ZAHB depends on the mass of the hydrogen-exhausted core at the time of ignition and on the mass in the overlying envelope. Those stars with lower mass, i.e., shallower envelopes, appear bluer because there is less mass to shield the hot hydrogen-burning shell. It is also possible for stars of very high mass, $M \gtrsim 12.0\,{\rm M}_{\odot}$, to reach high enough central temperatures on the HG for helium to ignite before reaching the GB. The 16.0-$\rm M_{\odot}$ star in Fig. 1 is such an example. As a result, these stars bypass the GB phase of evolution.

Evolution after the exhaustion of core-helium is very similar to evolution after core-hydrogen exhaustion at the end of the MS. The convective envelope deepens again, so that the star once more moves across towards the Hayashi track to begin what is called the asymptotic giant branch (AGB). On the AGB the star consists of a dense core composed of carbon and oxygen surrounded by a helium-burning shell which adds carbon to the degenerate core. Initially the hydrogen-burning shell is extinguished so that the luminosity is supplied exclusively by the helium-burning shell, characterizing the early AGB (EAGB) phase. If the star is massive enough the convective envelope can reach into the hydrogen-exhausted region again (second dredge-up). When the helium-burning shell catches up with the hydrogen-rich envelope, the hydrogen shell re-ignites and the two grow together, with the hydrogen-burning shell supplying most of the luminosity. During the following phase the helium shell is unstable, which can cause a helium shell flash in which the helium shell will suddenly release a large amount of luminosity. The energy released in the flash expands the star, resulting in the hydrogen shell cooling so much that it is extinguished. Convection once again reaches downward past the dead hydrogen shell. This mixes helium to the surface, as well as carbon that was mixed out of the helium shell by flash-driven convection. As the star subsequently contracts, the convection recedes and the hydrogen shell re-ignites but has now moved inwards in mass due to the envelope convection. This process is called the third dredge-up. The star continues its evolution up the

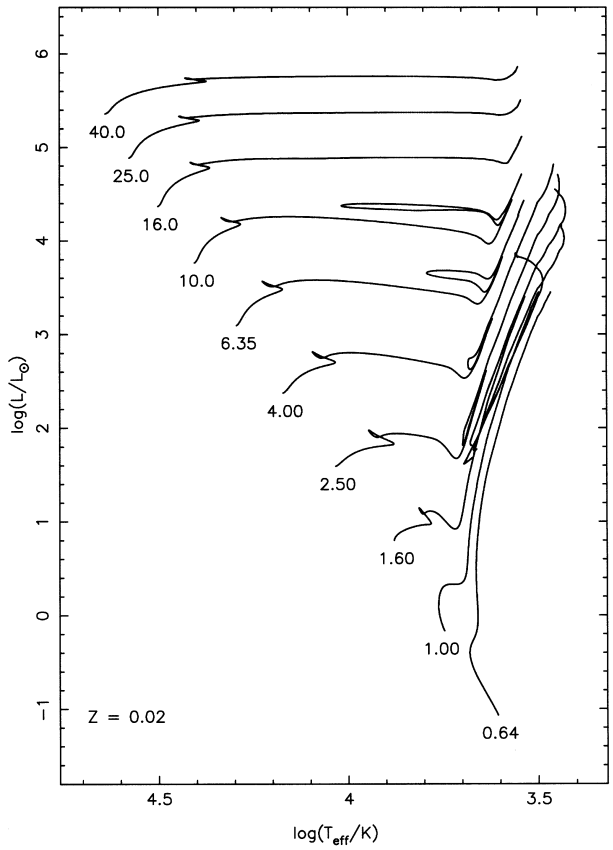

Figure 1. Selected OVS evolution tracks for $Z = 0.02$, for masses 0.64, 1.0, 1.6, 2.5, 4.0, 6.35, 10, 16, 25 and 40 $M_\odot$.

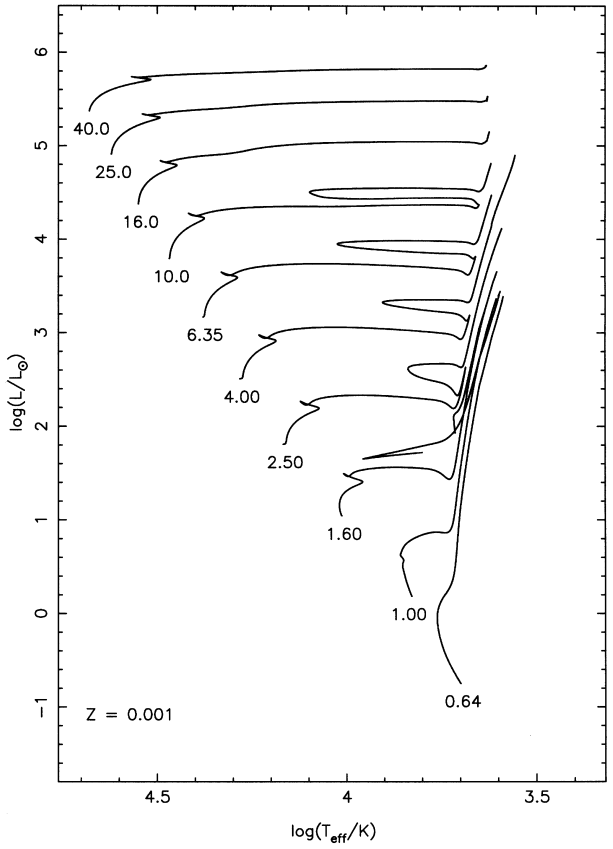

Figure 2. Same as Fig. 1 for $Z = 0.001$. The 1.0-$M_\odot$ post-helium flash track has been omitted for clarity.

AGB with the hydrogen shell producing almost all of the luminosity. The helium shell flash can repeat itself many times, and the cycle is known as a thermal pulse. This is the thermally pulsing asymptotic giant branch (TPAGB).

The stellar radius can grow to very large values on the AGB; this lowers the surface gravity of the star, so that the surface material is less tightly bound. Thus mass-loss from the stellar surface can become significant, with the rate of mass-loss actually accelerating with time during continued evolution up the AGB. Unfortunately, our understanding of the mechanisms that cause this mass-loss is poor, with possible suggestions linking it to the helium shell flashes or to periodic envelope pulsations. Whatever the cause, the influence on the evolution of AGB stars is significant. Mass-loss will eventually remove all of the stars envelope so that the hydrogen-burning shell shines through. The star then leaves the AGB and evolves to higher $T_{\rm eff}$ at nearly constant luminosity. As the photosphere gets hotter, the energetic photons become absorbed by the material which was thrown off while on the AGB. This causes the material to radiate, and the star may be seen as a planetary nebula. The core of the star then begins to fade as the nuclear burning ceases. The star is now a white dwarf (WD) and cools slowly at high temperature but low luminosity.

If the mass of the star is large enough, $M \gtrsim 7\,M_\odot$, the carbon-oxygen core is not degenerate and will ignite carbon as it contracts, followed by a succession of nuclear reaction sequences which very quickly produce an inner iron core. Any further reactions are endothermic and cannot contribute to the luminosity of the star. Photodisintegration of iron, combined with electron capture by protons and heavy nuclei, then removes most of the electron degeneracy pressure that was supporting the core, and it begins to collapse rapidly. When the density becomes large enough, the inner core rebounds, sending a shockwave outwards through the outer layers of the star that have remained suspended above the collapsing core. As a result, the envelope of the star is ejected in a supernova (SN) explosion, so that the AGB is effectively truncated at the start of carbon burning and the star has no TPAGB phase. The remnant in the inner core will stabilize to form a neutron star (NS) supported by neutron degeneracy pressure, unless the initial stellar mass is large enough that complete collapse to a black hole (BH) occurs.

Stars with $M \gtrsim 15\,M_\odot$ are severely affected by mass-loss during their entire evolution and may lose their envelopes during CHeB, or even on the HG, exposing nuclear processed material. If this occurs, then a naked helium star is produced and such stars, or stars about to become naked helium stars, may be Wolf–Rayet stars. Wolf–Rayet stars are massive objects which are found near the MS, are losing mass at very high rates, and show weak, or no, hydrogen lines in their spectra. Luminous blue variables (LBVs) are extremely massive post-MS objects with enormous mass-loss rates in a stage of evolution just prior to becoming Wolf–Rayet stars. Naked helium stars can also be produced from less massive stars in binaries as a consequence of mass transfer.

Variations in composition can also affect the stellar evolution time-scales as well as the appearance of the evolution on the HRD, and even the ultimate fate of the star. A more detailed discussion of the various phases of evolution can be found throughout this paper.

3 STELLAR MODELS

The fitting formulae are based on the stellar models computed by Pols et al. (1998). They computed a grid of evolution tracks for masses M between 0.5 and 50 $M_\odot$, and for seven values of metallicity, $Z = 0.0001$, 0.0003, 0.001, 0.004, 0.01, 0.02 and 0.03. They also considered the problem of enhanced mixing, such as overshooting beyond the classical boundary of convective instability. Its effect was modelled with a prescription based on a modification of the Schwarzschild stability criterion, introducing a free parameter δ_{ov} (which differs from the more commonly used parameter relating the overshooting distance to the pressure scaleheight; see Pols et al. 1998 for details). The tracks computed with a moderate amount of enhanced mixing (given by $\delta_{ov} = 0.12$ and labelled the OVS tracks by Pols et al. 1998) were found to best reproduce observations in a series of sensitive tests involving open clusters and ecliping binaries (see Schröder, Pols & Eggleton 1997 and Pols et al. 1997, 1998). We consequently use these OVS tracks as the data to which we fit our formulae.

For each Z, 25 tracks were computed, spaced by approximately 0.1 in $\log M$, except between 0.8 and 2.0 $M_\odot$ where four extra models were added to resolve the shape of the MS, which changes rapidly in this mass range. Hence we dispose of a data base of 175 evolution tracks, each containing several thousand individual models.

A subset of the resulting OVS tracks in the HRD are shown in Fig. 1 for $Z = 0.02$ and Fig. 2 for $Z = 0.001$. The considerable variation of model behaviour introduced by changes in metallicity is illustrated by Fig. 3. Detailed models of the same mass, $M = 6.35\,M_\odot$, are shown on the HRD for three different metallicities, $Z = 0.0001$, 0.001 and 0.02. Not only does a change in composition move the track to a different position in the HRD, but it also changes the appearance of each track, as can be seen by considering the extent of the hook feature towards the end of the MS and the blue loops during core helium burning. Furthermore, the $Z = 0.0001$ model ignites helium in its core while on the Hertzsprung gap, as opposed to the other models which evolve up the giant branch before reaching a high enough core temperature to start helium burning. In addition, the nuclear burning lifetime of a star can change by as much as a factor of 2 owing to differences in composition, as shown in Fig. 4 for a set of 2.5-$M_\odot$ models. This emphasizes the need to present the results of stellar evolution calculations for an extensive range of metallicity.

Mass-loss from stellar winds was neglected in the detailed stellar models, mainly because the mass-loss rates are uncertain by at least a factor of 3. We do include mass-loss in our analytic formulae in an elegant way, as will be described in Section 7.1, which allows us to experiment easily with different mass-loss rates and prescriptions.

4 PROCEDURE

We assign each evolution phase an integer type, k, where:

0 = MS star $M \lesssim 0.7$ deeply or fully convective
1 = MS star $M \gtrsim 0.7$
2 = Hertzsprung Gap (HG)
3 = First Giant Branch (GB)
4 = Core Helium Burning (CHeB)
5 = Early Asymptotic Giant Branch (EAGB)
6 = Thermally Pulsing Asymptotic Giant Branch (TPAGB)
7 = Naked Helium Star MS (HeMS)

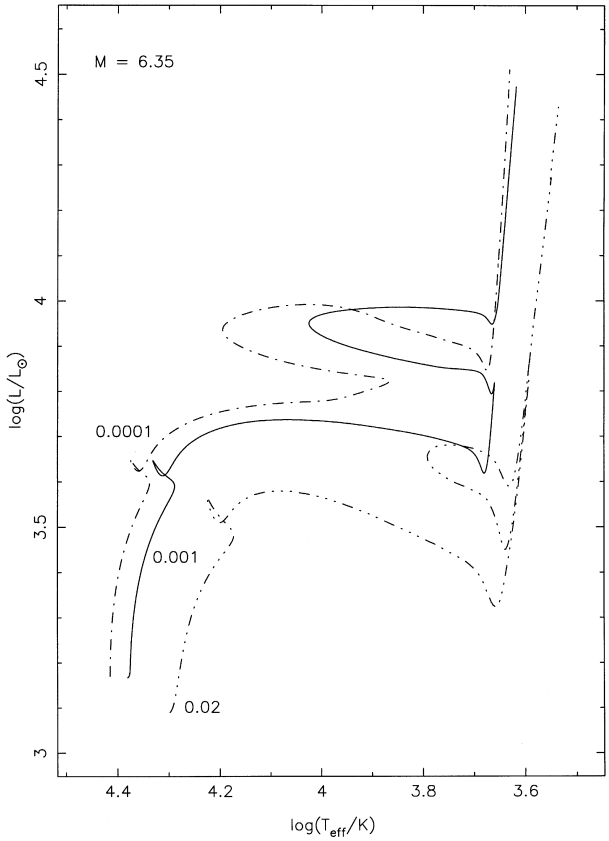

Figure 3. Detailed OVS evolution tracks for $M = 6.35\,M_\odot$, for metallicities 0.0001, 0.001 and 0.02.

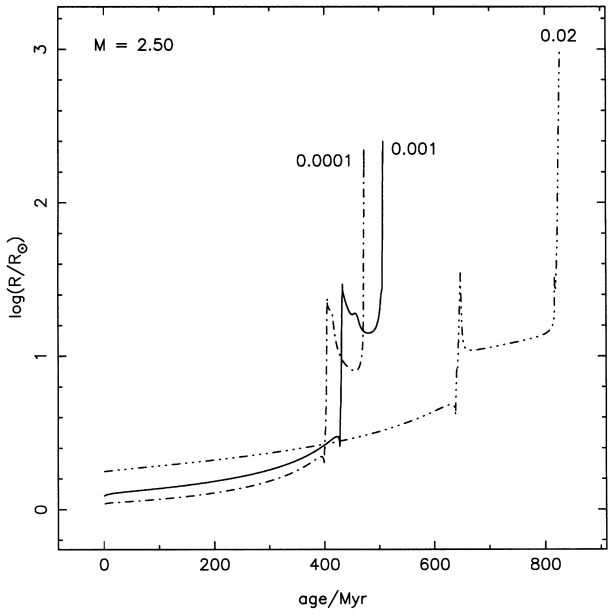

Figure 4. Radius evolution as a function of stellar age for $M = 2.5\,M_\odot$, for metallicities 0.0001, 0.001 and 0.02. Tracks are from the detailed models, and run from the ZAMS to the point of termination on the AGB.

8 = Naked Helium Star Hertzsprung Gap (HeHG)
9 = Naked Helium Star Giant Branch (HeGB)
10 = Helium White Dwarf (HeWD)
11 = Carbon/Oxygen White Dwarf (COWD)

12 = Oxygen/Neon White Dwarf (ONeWD)
13 = Neutron Star (NS)
14 = Black Hole (BH)
15 = massless remnant,

and we divide the MS into two phases to distinguish between deeply or fully convective low-mass stars and stars of higher mass with little or no convective envelope, as these will respond differently to mass-loss.

To begin with, we take different features of the evolution in turn, e.g., MS lifetime, ZAHB luminosity, and first try to fit them as $f(M)$ for a particular Z in order to get an idea of the functional form. We then extend the function to $g(M, Z)$, using $f(M)$ as a starting point. In this way we fit formulae to the end-points of the various evolutionary phases, as well as to the time-scales. We then fit the behaviour within each phase as $h(t, M, Z)$, e.g., $L_{\rm MS}(t, M, Z)$.

As a starting point we take the work of Tout et al. (1996), who fitted the zero-age main-sequence luminosity ($L_{\rm ZAMS}$) and radius ($R_{\rm ZAMS}$) as a function of M and Z. Their aim, as is ours, was to find simple computationally efficient functions which are accurate, continuous and differentiable in M and Z, such as rational polynomials. This is achieved using least-squares fitting to the data after choosing the initial functional form. In most cases we determine the type of function, the value of the powers, and the number of coefficients to be used, simply by inspecting the shape of the data; however, in some cases, such as the luminosity–core mass relation on the giant branch, the choice will be dictated by an underlying physical process. For the ZAMS, accuracy is very important because it fixes the star's position in the HRD. Tout et al. (1996) achieved $L_{\rm ZAMS}$ accurate to 3 per cent and $R_{\rm ZAMS}$ accurate to 1.2 per cent over the entire range. For the remainder of the functions we aim for rms errors less than 5 per cent and preferably a maximum individual error less than 5 per cent, although this has to be relaxed for some later stages of the evolution where the behaviour varies greatly with Z, but also where the model points are more uncertain owing to shortcomings in stellar evolution theory.

5 FITTING FORMULAE

In this section we present our formulae describing the evolution as a function of mass M and age t. The explicit Z-dependence is in most cases not given here, because it would clutter up the presentation. This Z-dependence is implicit whenever a coefficient of the form a_n or b_n appears in any of the formulae. The explicit dependence of these coefficients on Z is given in Appendix A. Coefficients of the form c_n, whose numerical values are given in this section, do not depend on Z.

We adopt the following unit conventions: numerical values of mass, luminosity and radius are in solar units, and values of time-scales and ages are in units of 10^6 yr, unless otherwise specified.

We begin by giving formulae for the most important critical masses, $M_{\rm hook}$ (the initial mass above which a hook appears in the MS), $M_{\rm HeF}$ (the maximum initial mass for which helium ignites degenerately in a helium flash) and $M_{\rm FGB}$ (the maximum initial mass for which helium ignites on the first giant branch). Values for these masses are given in table 1 of Pols et al. (1998), estimated from the detailed models for seven metallicities. These values can be accurately fitted as a function of Z by the following formulae, where $\zeta = \log(Z/0.02)$:

$$M_{\rm hook} = 1.0185 + 0.160\,15\zeta + 0.0892\zeta^2, \quad (1)$$

$$M_{\rm HeF} = 1.995 + 0.25\zeta + 0.087\zeta^2, \quad (2)$$

$$M_{\rm FGB} = \frac{13.048(Z/0.02)^{0.06}}{1 + 0.0012(0.02/Z)^{1.27}}. \quad (3)$$

Based on the last two critical masses, we make a distinction into three mass intervals, which will be useful in the later descriptions:

(i) low-mass (LM) stars, with $M < M_{\rm HeF}$, develope degenerate helium cores on the GB and ignite helium in a degenerate flash at the top of the GB;
(ii) intermediate-mass (IM) stars, with $M_{\rm HeF} \leq M \leq M_{\rm FGB}$, which evolve to the GB without developing degenerate helium cores, also igniting helium at the top of the GB, and
(iii) high-mass (HM) stars, with $M > M_{\rm FGB}$, ignite helium in the HG before the GB is reached, and consequently do not have a GB phase.

Note that this definition of IM and HM stars is different from the more often used one, based on whether or not carbon ignites non-degenerately.

5.1 Main sequence and Hertzsprung gap

To determine the base of the giant branch (BGB), we find where the mass of the convective envelope $M_{\rm CE}$ first exceeds a set fraction of the envelope mass $M_{\rm E}$ as $M_{\rm CE}$ increases in the HG. From inspection, the following fractions

$$M_{\rm CE} = \tfrac{2}{5}M_{\rm E} \quad M \lesssim M_{\rm HeF}$$

$$M_{\rm CE} = \tfrac{1}{3}M_{\rm E} \quad M \gtrsim M_{\rm HeF}$$

generally give a BGB point corresponding to the local minimum in luminosity at the start of the GB. We define helium ignition as the point where $L_{\rm He} = 0.01L$ for the first time. For HM stars this will occur before the BGB point is found, i.e., no GB, and thus we set $t_{\rm BGB} = t_{\rm HeI}$ for the sake of defining an end-point to the HG, so that BGB is more correctly the end of the HG (EHG), as this is true over the entire mass range.

The resultant lifetimes to the BGB are fitted as a function of M and Z by

$$t_{\rm BGB} = \frac{a_1 + a_2M^4 + a_3M^{5.5} + M^7}{a_4M^2 + a_5M^7}. \quad (4)$$

Fig. 5 shows how equation (4) fits the detailed model points for $Z = 0.0001$ and 0.03, which are the metallicities which lead to the largest errors. Over the entire metallicity range the function gives an rms error of 1.9 per cent and a maximum error of 4.8 per cent. In order that the time spent on the HG will always be a small fraction of the time taken to reach the BGB, even for LM stars which do not have a well-defined HG, the MS lifetimes are taken to be

$$t_{\rm MS} = \max(t_{\rm hook}, xt_{\rm BGB}), \quad (5)$$

where $t_{\rm hook} = \mu t_{\rm BGB}$ and

$$x = \max(0.95,\ \min[0.95 - 0.03(\zeta + 0.30103),\ \ 0.99]) \quad (6)$$

$$\mu = \max\left[0.5,\ \ 1.0 - 0.01\max\left(\frac{a_6}{M^{a_7}},\ \ a_8 + \frac{a_9}{M^{a_{10}}}\right)\right]. \quad (7)$$

Note that μ is ineffective for $M < M_{\rm hook}$, i.e., stars without a hook feature, and in this case the functions ensure that $x > \mu$.

So we now have defined the time at the end of the MS, $t_{\rm MS}$, and the time taken to reach the start of the GB (or end of the HG),

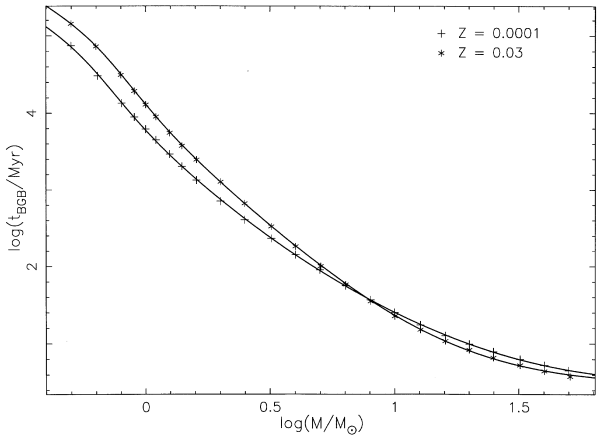

Figure 5. Time taken to reach the base of the giant branch as a function of stellar mass as given by equation (4), shown against the detailed model points, for $Z = 0.0001$ and 0.03 which give the worst fit of all the metallicities. The maximum error over the entire metallicity range is 4.8 per cent, and the rms error is 1.9 per cent.

$t_{\rm BGB}$, such that

$t : 0.0 \rightarrow t_{\rm MS}$ MS evolution

$t : t_{\rm MS} \rightarrow t_{\rm BGB}$ HG evolution.

The starting values for L and R are the ZAMS points fitted by Tout et al. (1996). We fit the values at the end of the MS, $L_{\rm TMS}$ and $R_{\rm TMS}$, as well as at the end of the HG,

$$L_{\rm EHG} = \begin{cases} L_{\rm BGB} & M < M_{\rm FGB} \\ L_{\rm HeI} & M \geq M_{\rm FGB} \end{cases}$$

$$R_{\rm EHG} = \begin{cases} R_{\rm GB}(L_{\rm BGB}) & M < M_{\rm FGB} \\ R_{\rm HeI} & M \geq M_{\rm FGB} \end{cases}.$$

The luminosity at the end of the MS is approximated by

$$L_{\rm TMS} = \frac{a_{11}M^3 + a_{12}M^4 + a_{13}M^{a_{16}+1.8}}{a_{14} + a_{15}M^5 + M^{a_{16}}}, \tag{8}$$

with $a_{16} \approx 7.2$. This proved fairly straightforward to fit, but the behaviour of $R_{\rm TMS}$ is not so smooth and thus requires a more complicated function in order to fit it continuously. The resulting fit is

$$R_{\rm TMS} = \frac{a_{18} + a_{19}M^{a_{21}}}{a_{20} + M^{a_{22}}} \quad M \leq a_{17} \tag{9a}$$

$$R_{\rm TMS} = \frac{c_1M^3 + a_{23}M^{a_{26}} + a_{24}M^{a_{26}+1.5}}{a_{25} + M^5} M \geq M_*, \tag{9b}$$

with straight-line interpolation to connect equations (9a) and (9b) between the end-points, where

$$M_* = a_{17} + 0.1, \quad 1.4 \leq a_{17} \leq 1.6,$$

and $c_1 = -8.672\,073 \times 10^{-2}$, $a_{21} \approx 1.5$, $a_{22} \approx 3.1$ and $a_{26} \approx 5.5$. Note that for low masses, $M < 0.5$, where the function is being extrapolated we add the condition

$$R_{\rm TMS} = \max(R_{\rm TMS}, 1.5R_{\rm ZAMS})$$

to avoid possible trouble in the distant future.

The luminosity at the base of the GB is approximated by

$$L_{\rm BGB} = \frac{a_{27}M^{a_{31}} + a_{28}M^{c_2}}{a_{29} + a_{30}M^{c_3} + M^{a_{32}}}, \tag{10}$$

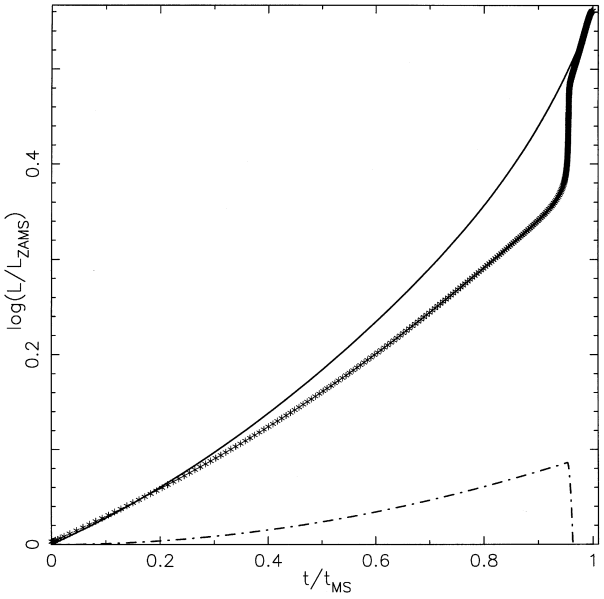

Figure 6. Luminosity evolution on the main sequence for a typical detailed model with a hook feature (star points) decomposed into two functions: a smooth polynomial (solid line) and a pertubation function (dot-dashed line).

with $c_2 = 9.301\,992$, $c_3 = 4.637\,345$, $a_{31} \approx 4.6$ and $a_{32} \approx 6.7$. The description of $L_{\rm HeI}$, $R_{\rm GB}$ and $R_{\rm HeI}$ is given in later sections.

5.1.1 *Main-sequence evolution*

On the MS we define a fractional time-scale

$$\tau = \frac{t}{t_{\rm MS}}. \tag{11}$$

As a star evolves across the MS, its evolution accelerates so that it is possible to model the time dependence of the logarithms of the luminosity and radius by polynomials in τ. Luminosity is given by

$$\log\frac{L_{\rm MS}(t)}{L_{\rm ZAMS}} = \alpha_L\tau + \beta_L\tau^\eta + \left(\log\frac{L_{\rm TMS}}{L_{\rm ZAMS}} - \alpha_L - \beta_L\right)\tau^2 - \Delta L(\tau_1^2 - \tau_2^2) \tag{12}$$

and radius by

$$\log\frac{R_{\rm MS}(t)}{R_{\rm ZAMS}} = \alpha_R\tau + \beta_R\tau^{10} + \gamma\tau^{40} + \left(\log\frac{R_{\rm TMS}}{R_{\rm ZAMS}} - \alpha_R - \beta_R - \gamma\right)\tau^3 - \Delta R(\tau_1^3 - \tau_2^3), \tag{13}$$

where

$$\tau_1 = \min(1.0, t/t_{\rm hook}) \tag{14}$$

$$\tau_2 = \max\left\{0.0, \min\left[1.0, \frac{t - (1.0 - \epsilon)t_{\rm hook}}{\epsilon t_{\rm hook}}\right]\right\} \tag{15}$$

for $\epsilon = 0.01$.

We add ΔL and ΔR as pertubations to the smooth polynomial evolution of L and R in order to mimic the hook behaviour for $M > M_{\rm hook}$. In effect, we have

$$L_{\rm MS}(t) = L_a(t)/L_b(t),$$

where $L_a(t)$ is a smooth function describing the long-term behaviour of $L_{\rm MS}(t)$, and $L_b(t)$ is another smooth function describing short-term pertubations where

$$\log L_b(t) = \Delta L(\tau_1^2 - \tau_2^2),$$

and the action of τ_2 achieves a smooth transition over $\Delta t = \epsilon t_{\rm hook}$. This decomposition of $L(t)$ into $L_a(t)$ and $L_b(t)$ for a typical detailed model is illustrated by Fig. 6. The luminosity pertubation is approximated by

$$\Delta L = \begin{cases} 0.0 & M \le M_{\rm hook} \\ B\left(\dfrac{M - M_{\rm hook}}{a_{33} - M_{\rm hook}}\right)^{0.4} & M_{\rm hook} < M < a_{33} \\ \min\left(\dfrac{a_{34}}{M^{a_{35}}}, \dfrac{a_{36}}{M^{a_{37}}}\right) & M \ge a_{33} \end{cases} \quad (16)$$

where $B = \Delta L(a_{33})$, $1.25 \le a_{33} \le 1.6$, $a_{35} \approx 0.4$ and $a_{37} \approx 0.6$.

The radius pertubation is approximated by

$$\Delta R = \begin{cases} 0.0 & M \le M_{\rm hook} \\ a_{43}\left(\dfrac{M - M_{\rm hook}}{a_{42} - M_{\rm hook}}\right)^{0.5} & M_{\rm hook} < M \le a_{42} \\ a_{43} + (B - a_{43})\left(\dfrac{M - a_{42}}{2.0 - a_{42}}\right)^{a_{44}} & a_{42} < M < 2.0 \\ \dfrac{a_{38} + a_{39}M^{3.5}}{a_{40}M^3 + M^{a_{41}}} - 1.0 & M \ge 2.0, \end{cases} \quad (17)$$

where $B = \Delta R(M = 2.0)$, $a_{41} \approx 3.6$, $1.1 \le a_{42} \le 1.25$ and $a_{44} \approx 1.2$.

The exponent $\eta = 10$ in equation (12), unless $Z \le 0.0009$ when it is given by

$$\eta = \begin{cases} 10 & M \le 1.0 \\ 20 & M \ge 1.1, \end{cases} \quad (18)$$

with linear interpolation between the mass limits.

The remaining functions for this section are those that describe the behaviour of the coefficients in equations (12) and (13). The fact that these can appear messy and complicated in places reflects rapid changes in the shape of the L and R evolution for the detailed models as a function of M as well as Z. This is illustrated in Figs 7, 8, 9 and 10, which also show the tracks derived from these functions, exhibiting that our efforts have not been in vain. The fitting of the coefficients is also complicated by the sensitivity of equations (12) and (13) to small changes in the values of the coefficients. Ideally, we would like all the functions to be smooth and differentiable across the entire parameter space, but in some places this has to be sacrificed to ensure that the position of all the fitted tracks on the HRD is as accurate as possible. This is deemed necessary as the main use of the functions is envisaged to be the simulation of colour–magnitude diagrams for comparison with observations.

The luminosity α coefficient is approximated by

$$\alpha_{\rm L} = \frac{a_{45} + a_{46}M^{a_{48}}}{M^{0.4} + a_{47}M^{1.9}} \qquad M \ge 2.0, \quad (19a)$$

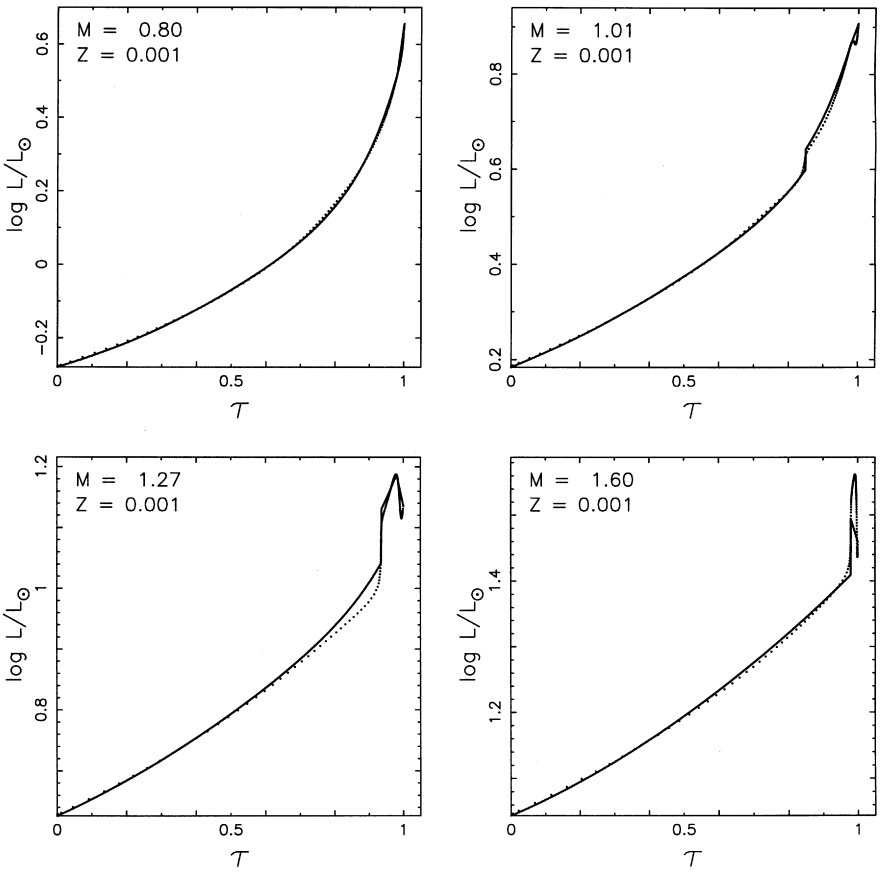

Figure 7. Luminosity evolution on the main sequence as given by equation (12) (solid line) and from the detailed models (points) for selected masses with a metallicity of 0.001.

where $a_{48} \approx 1.6$, and then

$$\alpha_L = \begin{cases} a_{49} & M < 0.5 \\ a_{49} + 5.0(0.3 - a_{49})(M - 0.5) & 0.5 \le M < 0.7 \\ 0.3 + (a_{50} - 0.3)(M - 0.7)/(a_{52} - 0.7) & 0.7 \le M < a_{52} \\ a_{50} + (a_{51} - a_{50})(M - a_{52})/(a_{53} - a_{52}) & a_{52} \le M < a_{53} \\ a_{51} + (B - a_{51})(M - a_{53})/(2.0 - a_{53}) & a_{53} \le M < 2.0, \end{cases} \quad (19b)$$

where $B = \alpha_L(M = 2.0)$, $1.0 \le a_{52} \le 1.1$ and $1.1 \le a_{53} \le 1.25$.

The luminosity β coefficient is approximated by

$$\beta_L = \max(0.0,\ a_{54} - a_{55}M^{a_{56}}), \quad (20)$$

where $a_{56} \approx 0.96$. Then, if $M > a_{57}$ and $\beta_L > 0.0$,

$$\beta_L = \max(0.0, B - 10.0(M - a_{57})B),$$

where $B = \beta_L(M = a_{57})$ and $1.25 \le a_{57} \le 1.6$.

The radius α coefficient is approximated by

$$\alpha_R = \frac{a_{58}M^{a_{60}}}{a_{59} + M^{a_{61}}} \qquad a_{66} \le M \le a_{67}, \quad (21a)$$

where $a_{60} \approx 1.8$ and $a_{61} \approx 2.3$, and then

$$\alpha_R = \begin{cases} a_{62} & M < 0.5 \\ a_{62} + (a_{63} - a_{62})(M - 0.5)/0.15 & 0.5 \le M < 0.65 \\ a_{63} + (a_{64} - a_{63})(M - 0.65)/(a_{68} - 0.65) & 0.65 \le M < a_{68} \\ a_{64} + (B - a_{64})(M - a_{68})/(a_{66} - a_{68}) & a_{68} \le M < a_{66} \\ C + a_{65}(M - a_{67}) & a_{67} < M, \end{cases} \quad (21b)$$

where $B = \alpha_R(M = a_{66})$, $C = \alpha_R(M = a_{67})$, $0.8 \le a_{66} \le 1.6$, $3.5 \le a_{67} \le 7.2$ and $0.8 \le a_{66} \le 1.0$.

The radius β coefficient is approximated by $\beta_R = \beta'_R - 1$, where

$$\beta'_R = \frac{a_{69}M^{3.5}}{a_{70} + M^{a_{71}}} \qquad 2.0 \le M \le 16.0, \quad (22a)$$

with $a_{71} \approx 3.5$ and $1.4 \le a_{74} \le 1.6$, and then

$$\beta'_R = \begin{cases} 1.06 & M \le 1.0 \\ 1.06 + (a_{72} - 1.06)(M - 1.0)/(a_{74} - 1.06) & 1.0 < M < a_{74} \\ a_{72} + (B - a_{72})(M - a_{74})/(2.0 - a_{74}) & a_{74} \le M < 2.0 \\ C + a_{73}(M - 16.0) & 16.0 < M \end{cases} \quad (22b)$$

where $B = \beta'_R(M = 2.0)$, $C = \beta'_R(M = 16.0)$.

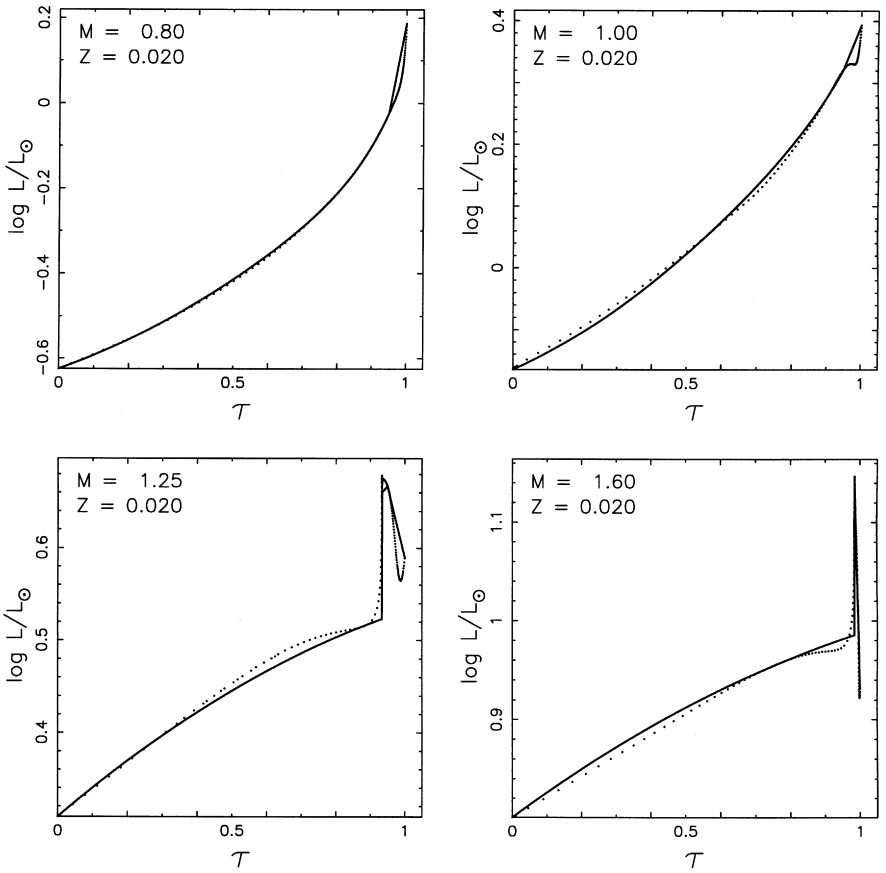

Figure 8. Same as Fig. 7 for $Z = 0.02$.

If $M > a_{75} + 0.1$, then $\gamma = 0.0$, where $1.0 \leq a_{75} \leq 1.6$. Otherwise

$$\gamma = \begin{cases} a_{76} + a_{77}(M - a_{78})^{a_{79}} & M \leq 1.0 \\ B + (a_{80} - B)\left(\dfrac{M - 1.0}{a_{75} - 1.0}\right)^{a_{81}} & 1.0 < M \leq a_{75} \\ C - 10.0(M - a_{75})C & a_{75} < M < a_{75} + 0.1, \end{cases} \tag{23}$$

where $a_{79} \approx 9.4$, $a_{81} \approx 2.5$, $B = \gamma(M = 1.0)$ and $C = a_{80}$, unless $a_{75} = 1.0$ when $C = B$.

Following Tout et al. (1997), we note that low-mass MS stars can be substantially degenerate below about $0.1\,\mathrm{M}_\odot$, so we take

$$R_{\mathrm{MS}} = \max[R_{\mathrm{MS}}, 0.0258(1.0 + X)^{5/3}\,\mathrm{M}^{-1/3}] \tag{24}$$

for such stars, where $X = 0.76 - 3.0Z$ is the initial hydrogen abundance (Pols et al. 1998).

5.1.2 *Hertzsprung-gap evolution*

During the HG we define

$$\tau = \frac{t - t_{\mathrm{MS}}}{t_{\mathrm{BGB}} - t_{\mathrm{MS}}}. \tag{25}$$

Then for the luminosity and radius we simply take

$$L_{\mathrm{HG}} = L_{\mathrm{TMS}}\left(\frac{L_{\mathrm{EHG}}}{L_{\mathrm{TMS}}}\right)^{\tau} \tag{26}$$

$$R_{\mathrm{HG}} = R_{\mathrm{TMS}}\left(\frac{R_{\mathrm{EHG}}}{R_{\mathrm{TMS}}}\right)^{\tau}. \tag{27}$$

On the MS we do not consider the core to be dense enough with respect to the envelope to actually define a core mass, i.e., $M_{\mathrm{c,MS}} = 0.0$. The core mass at the end of the HG is

$$M_{\mathrm{c,EHG}} = \begin{cases} M_{\mathrm{c,GB}}(L = L_{\mathrm{BGB}}) & M < M_{\mathrm{HeF}} \\ M_{\mathrm{c,BGB}} & M_{\mathrm{HeF}} \leq M < M_{\mathrm{FGB}} \\ M_{\mathrm{c,HeI}} & M \geq M_{\mathrm{FGB}}, \end{cases} \tag{28}$$

where $M_{\mathrm{c,GB}}$, $M_{\mathrm{c,BGB}}$ and $M_{\mathrm{c,HeI}}$ will be defined in Sections 5.2 and 5.3. At the beginning of the HG we set $M_{\mathrm{c,TMS}} = \rho M_{\mathrm{c,EHG}}$, where

$$\rho = \frac{1.586 + M^{5.25}}{2.434 + 1.02M^{5.25}}, \tag{29}$$

and simply allow the core mass to grow linearly with time so that

$$M_{\mathrm{c,HG}} = [(1 - \tau)\rho + \tau]M_{\mathrm{c,EHG}}. \tag{30}$$

If the HG star is losing mass (as described in Section 7.1), it is necessary to take $M_{\mathrm{c,HG}}$ as the maximum of the core mass at the previous time-step and the value given by equation (30).

5.2 First giant branch

The evolution along the first giant branch (GB) can be modelled, following Eggleton et al. (1989), using a power-law

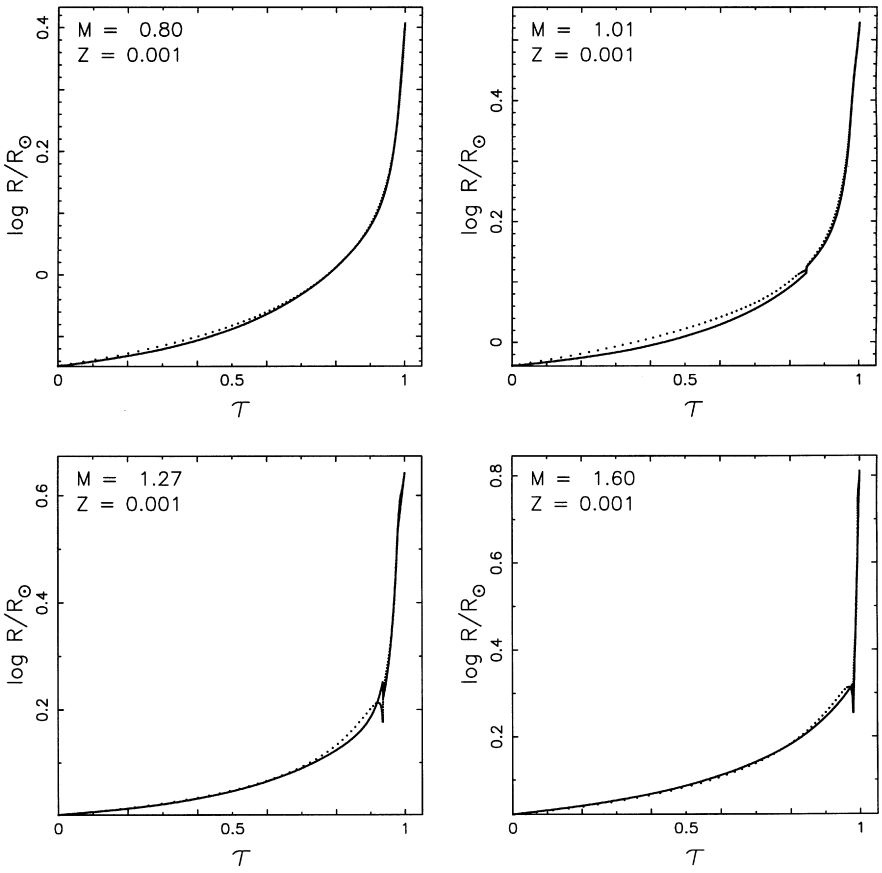

Figure 9. Radius evolution on the main sequence as given by equation (13) (solid line) and from the detailed models (points) for selected masses with a metallicity of 0.001.

core mass–luminosity relation,

$$L = DM_{\rm c}^{p}. \tag{31}$$

The evolution is then determined by the growth of the core mass as a result of hydrogen burning which, in a state of thermal equilibrium, is given by

$$L = EX_{\rm e}\dot{M}_{\rm c} \Rightarrow \dot{M}_{\rm c} = A_{\rm H}L, \tag{32}$$

where

$X_{\rm e}$ = envelope mass fraction of hydrogen,

E = the specific energy release and

$A_{\rm H}$ = hydrogen rate constant.

Thus

$$\frac{{\rm d}M_{\rm c}}{{\rm d}t} = A_{\rm H}DM_{\rm c}^{p}, \tag{33}$$

which upon integration gives

$$M_{\rm c} = [(p-1)A_{\rm H}D(t_{\rm inf} - t)]^{\frac{1}{1-p}} \tag{34}$$

or

$$L = D[(p-1)A_{\rm H}D(t_{\rm inf} - t)]^{\frac{p}{1-p}}, \tag{35}$$

so that the time evolution of either $M_{\rm c}$ or L is given and we can then simply find the other from the $M_{\rm c}$–L relation. Also, when $L = L_{\rm BGB}$ we have $t = t_{\rm BGB}$, which defines the integration constant

$$t_{\rm inf} = t_{\rm BGB} + \frac{1}{{\rm A_H}D(p-1)}\left(\frac{D}{L_{\rm BGB}}\right)^{\frac{p-1}{p}}. \tag{36}$$

Now, as noted in Tout et al. (1997), the single power law $L \propto M_{\rm c}^{6}$ is a good approximation to the evolution for small $M_{\rm c}$, but the relation flattens out as $M_{\rm c}$ approaches the Chandrasekhar mass $M_{\rm Ch}$. They expanded the relation to consist of two power-law parts. We use an improved form which, albeit somewhat more ad hoc, follows much better the actual time evolution along the GB. Our $M_{\rm c}$–L relation has the form

$$L = \min(BM_{\rm c}^{q}, DM_{\rm c}^{p}) \qquad (q < p), \tag{37}$$

so that the first part describes the high-luminosity end and the second the low-luminosity end of the relation, with the two crossing at

$$M_x = \left(\frac{B}{D}\right)^{\frac{1}{p-q}}. \tag{38}$$

The parameters B, D, p and q are constants in time for each model, and indeed are constant in mass for $M < M_{\rm HeF}$. For $M \geq M_{\rm HeF}$ it is necessary to introduce a dependence on initial mass so that we actually have a $M_{\rm c}$–L–M relation. The only region in the $M_{\rm c}$–L parameter space where we find that a Z-dependence is required is in the value of D for $M < M_{\rm HeF}$. The parameters are

$$p = \begin{cases} 6 & M \leq M_{\rm HeF} \\ 5 & M \geq 2.5 \end{cases}$$

$$q = \begin{cases} 3 & M \leq M_{\rm HeF} \\ 2 & M \geq 2.5 \end{cases}$$

$$B = \max(3\times10^{4}, 500 + 1.75\times10^{4}M^{0.6})$$

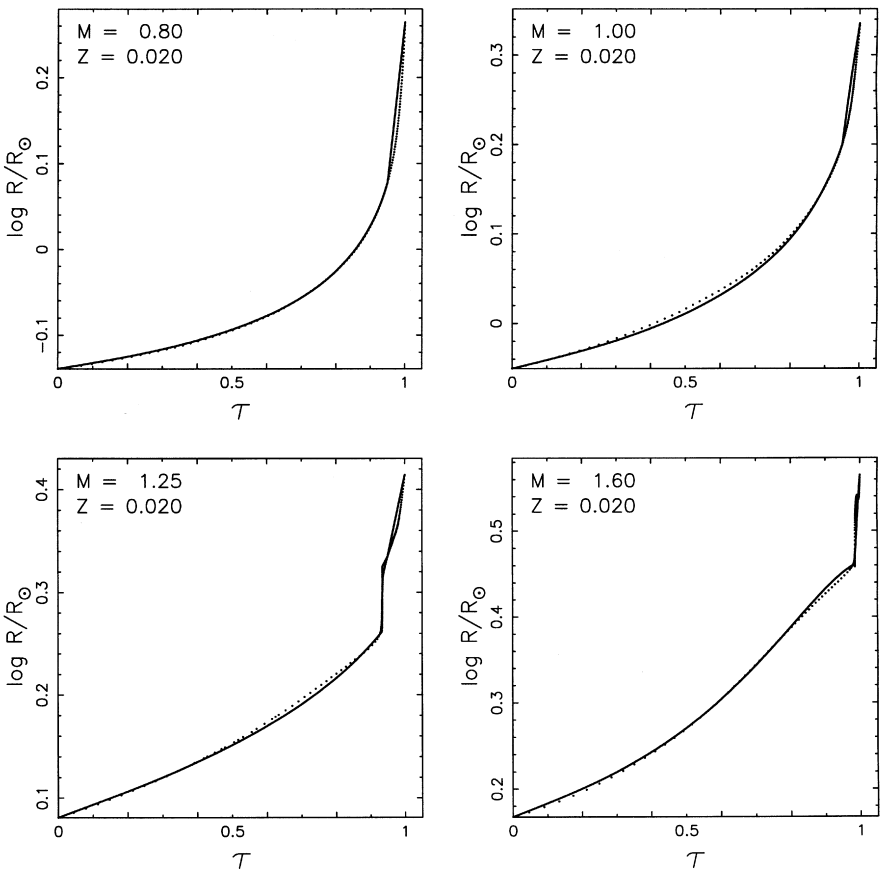

Figure 10. Same as Fig. 9 for $Z = 0.02$.

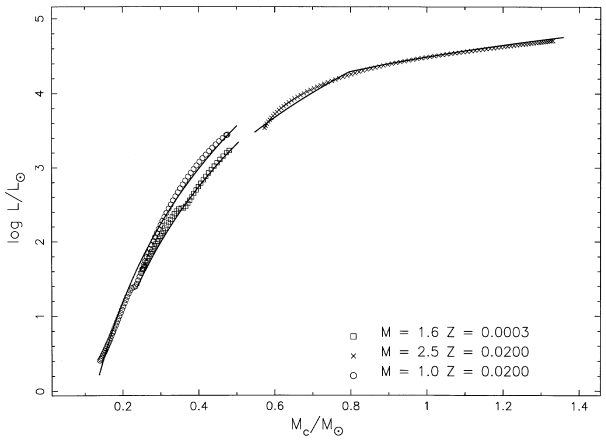

Figure 11. Relation between core mass and luminosity on the giant branch, showing the fit to points taken from selected detailed models given by equation (37) (solid lines).

$$\log D = \begin{cases} 5.37 + 0.135\zeta \quad [= D_0] & M \le M_{\rm HeF} \\ \max(-1.0, 0.975D_0 - 0.18M, 0.5D_0 - 0.06M) & \\ & M \ge 2.5 \end{cases}$$

with linear interpolation over the transition region, $M_{\rm HeF} < M < 2.5$, in order to keep the parameters continuous in M. Thus isochrones constructed with these functions will not give a discontinuity on the GB. The behaviour of equation (37) is shown in Fig. 11 as the fit to selected model points (note how the relation flattens out as the luminosity increases).

Equation (34) now becomes

$$M_{\rm c,GB} = \begin{cases} [(p-1)A_{\rm H}D(t_{\rm inf,1} - t)]^{\frac{1}{1-p}} & t \le t_x \\ [(q-1)A_{\rm H}B(t_{\rm inf,2} - t)]^{\frac{1}{1-q}} & t > t_x \end{cases} \tag{39}$$

for $t_{\rm BGB} \le t \le t_{\rm HeI}$, where

$$t_{\rm inf,1} = t_{\rm BGB} + \frac{1}{(p-1)A_{\rm H}D}\left(\frac{D}{L_{\rm BGB}}\right)^{\frac{p-1}{p}} \tag{40}$$

$$t_x = t_{\rm inf,1} - (t_{\rm inf,1} - t_{\rm BGB})\left(\frac{L_{\rm BGB}}{L_x}\right)^{\frac{p-1}{p}} \tag{41}$$

$$t_{\rm inf,2} = t_x + \frac{1}{(q-1)A_{\rm H}B}\left(\frac{B}{L_x}\right)^{\frac{q-1}{q}}. \tag{42}$$

The GB ends at $t = t_{\rm HeI}$, corresponding to $L = L_{\rm HeI}$ (see Section 5.3), given by

$$t_{\rm HeI} = \begin{cases} t_{\rm inf,1} - \dfrac{1}{(p-1)A_{\rm H}D}\left(\dfrac{D}{L_{\rm HeI}}\right)^{\frac{p-1}{p}} & L_{\rm HeI} \le L_x \\ t_{\rm inf,2} - \dfrac{1}{(q-1)A_{\rm H}B}\left(\dfrac{B}{L_{\rm HeI}}\right)^{\frac{q-1}{q}} & L_{\rm HeI} > L_x \end{cases}. \tag{43}$$

The value used for $A_{\rm H}$ depends on whether we take the PP chain or the CNO cycle as the hydrogen-burning mechanism, with the CNO cycle being the more likely on the GB. Now

$$E = \epsilon_{\rm CNO}/m(He^4) \approx 6.018 \times 10^{18}\,{\rm erg\,g^{-1}};$$

Table 1. A selection of values for the mass-dependent hydrogen rate constant, with approximate time-scales also listed.

M	$\log A'_{\rm H}$	$\frac{t_{\rm HeI} - t_{\rm BGB}}{t_{\rm BGB}}$	$t_{\rm BGB}$/Myr
1.0	−4.8	6.4×10^{-2}	10^4
2.0	−4.1	2.0×10^{-2}	10^3
5.0	−3.4	2.4×10^{-3}	10^2

thus

$$A_{\rm H} = (EX_{\rm e})^{-1} = 2.373\,83 \times 10^{-19}\,{\rm g\,erg^{-1}}$$

$$\Rightarrow \; A_{\rm H} \approx 1.44 \times 10^{-5}\,{\rm M_\odot\,L_\odot^{-1}\,Myr^{-1}},$$

i.e., $\log A_{\rm H} = -4.84$. In practice, there are small deviations from thermal equilibrium which increase with stellar mass. As the value of $A_{\rm H}$ fixes the rate of evolution on the GB and thus the GB time-scale, it is important for it to be accurate, especially if we want to use the formulae for population synthesis. We find that the detailed models are best represented if we introduce a mass-dependent $A_{\rm H}$, i.e., $A'_{\rm H}$, where

$$\log A'_{\rm H} = \max[-4.8, \min(-5.7 + 0.8M, -4.1 + 0.14M)].$$

Some representative values of $A'_{\rm H}$ as a function of initial stellar mass are shown in Table 1, along with approximate values for the GB lifetime and the time taken to reach the GB.

Evolution on the GB actually falls into two fairly distinct categories depending on whether the initial mass of the star is greater than or less than $M_{\rm HeF}$. If $M < M_{\rm HeF}$, then the star has a degenerate helium core on the GB, which grows according to the $M_{\rm c,GB}$ relation derived from equation (37). When helium ignites at the tip of the GB, it does so degenerately resulting in the helium flash. However, for IM stars on the GB, $M \ge M_{\rm HeF}$, the helium core is non-degenerate and the relative time spent on the GB is much shorter, and thus the models show that $M_{\rm c,GB}$ is approximately constant from the BGB to HeI. In this case we still use all the above equations to calculate the time-scales and the luminosity evolution, but the corresponding value of $M_{\rm c}$ is a dummy variable. The actual core mass at the BGB is given by a mass-dependent formula

$$M_{\rm c,BGB} = \min[0.95M_{\rm c,BAGB}, (C + c_1 M^{c_2})^{\frac{1}{4}}], \tag{44}$$

with $C = M_{\rm c}[L_{\rm BGB}(M_{\rm HeF})]^4 - c_1 M_{\rm HeF}^{c_2}$, ensuring that the formula is continuous with the $M_{\rm c}$–L relation at $M = M_{\rm HeF}$, and $M_{\rm c,BAGB}$ given by equation (66). The constants $c_1 = 9.209\,25 \times 10^{-5}$ and $c_2 = 5.402\,216$ are independent of Z, so that for large enough M we have $M_{\rm c,BGB} \approx 0.098M^{1.35}$, independent of Z. Thus, on the GB we simply take

$$M_{\rm c,GB} = M_{\rm c,BGB} + (M_{\rm c,HeI} - M_{\rm c,BGB})\tau \quad M \ge M_{\rm HeF}, \tag{45}$$

with

$$\tau = \frac{t - t_{\rm BGB}}{t_{\rm HeI} - t_{\rm BGB}}$$

to account for the small growth of the non-degenerate core, while $M_{\rm c,GB}$ is given by equation (39) for $M < M_{\rm HeF}$. $M_{\rm c,HeI}$ is described in Section 5.3.

Furthermore, as giants have a deep convective envelope and thus lie close to the Hayashi track, we can find the radius as a function of L and M,

$$R_{\rm GB} = A(L^{b_1} + b_2 L^{b_3}), \tag{46}$$

where

$$A = \min(b_4 M^{-b_5}, b_6 M^{-b_7}),$$

and $b_1 \approx 0.4$, $b_2 \approx 0.5$ and $b_3 \approx 0.7$. A useful quantity is the exponent x to which R depends on M at constant L, $R_{\rm GB} \propto M^{-x}$. Thus we also fit x across the entire mass range by $A = bM^{-x}$, i.e., a hybrid of b_5 and b_7, to give

$$x = 0.304\,06 + 0.0805\zeta + 0.0897\zeta^2 + 0.0878\zeta^3 + 0.0222\zeta^4, \tag{47}$$

so that it can be used if required. Thus for $Z = 0.02$, as an example, we have

$$R_{\rm GB} \approx 1.1 M^{-0.3}(L^{0.4} + 0.383 L^{0.76}). \tag{48}$$

Fig. 12 exhibits the accuracy of equation (46) for solar-mass models of various metallicity.

5.3 Core helium burning

The behaviour of stellar models in the HRD during CHeB is fairly complicated and depends strongly on the mass and metallicity. For LM stars, helium ignites at the top of the GB and CHeB corresponds to the horizontal branch (including the often observed red clump); the transition between the helium flash and the start of steady CHeB at the ZAHB is very rapid, and we take it to be instantaneous. For IM stars, CHeB can be roughly divided in two phases, namely descent along the GB to a minimum luminosity, followed by a blue loop excursion to higher $T_{\rm eff}$ connecting back up to the base of the AGB (BAGB). However, not all IM stars exhibit a blue loop, in some cases staying close to the GB throughout CHeB (the so-called 'failed blue loop'). Sometimes the blue loop is also followed by another period of CHeB on the GB, but this is usually much shorter than the first phase and we choose to ignore it. For HM stars, helium ignites in the HG and CHeB also consists of two phases, namely a blue phase before reaching the GB, followed by a red (super)giant phase.

For the purpose of modelling, we define the blue phase of CHeB as that part which is not spent on the giant branch. This means that the position in the HRD during the blue phase can in fact be quite red, e.g., it includes the red clump and failed blue loops. By definition, for the LM regime the whole of CHeB is blue. For IM stars, the blue phase comes after the RG phase, while for HM stars it precedes the RG phase.

The transition between the LM and IM star regime occurs over a small mass range (a few times $0.1\,{\rm M}_\odot$), but it can be modelled in a continuous way with a factor of the form $1 + \alpha \exp 15(M - M_{\rm HeF})$ in the LM formulae (see below). With α of order unity, this factor can be neglected if $M \ll M_{\rm HeF}$. We also require continuity of LM CHeB stars with naked helium stars when the envelope mass goes to zero. The formulae are also continuous between IM and HM stars for $Z \leq 0.002$. For higher Z, however, there is a discontinuity in the CHeB formulae at $M = M_{\rm FGB}$, because the transition becomes too complicated to model continuously while keeping the formulae simple.

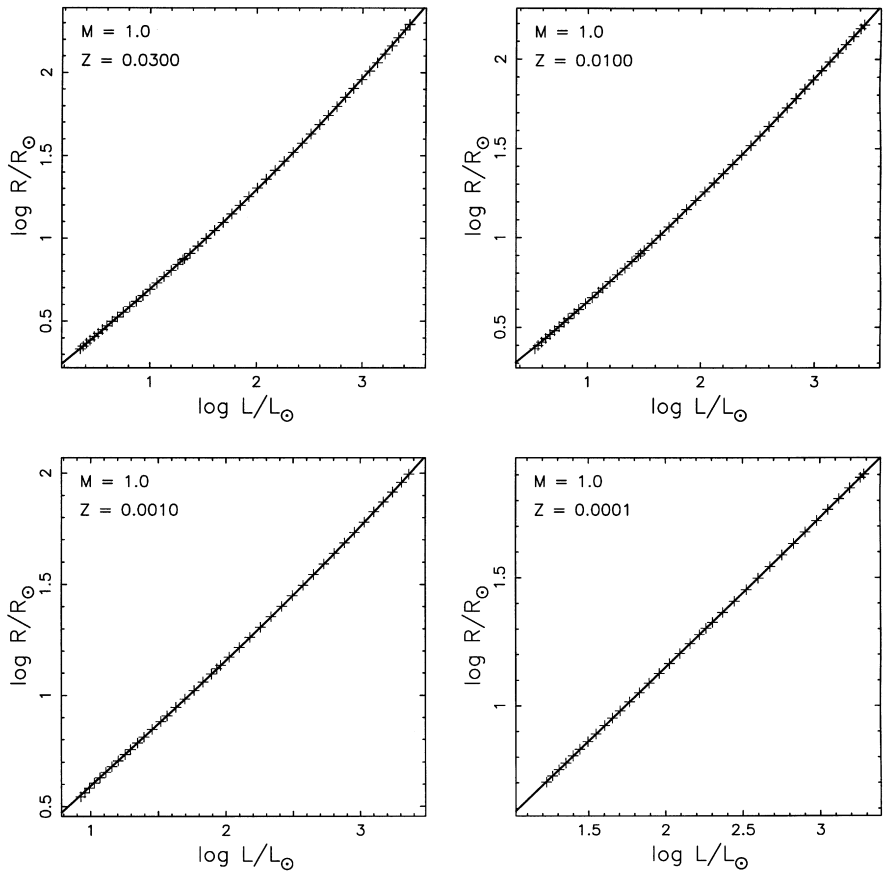

Figure 12. Relation between radius and luminosity on the giant branch as given by equation (46) (solid line) and from the detailed models (crosses) for $1.0\,{\rm M}_\odot$ at various metallicities.

The luminosity at helium ignition is approximated by

$$L_{\rm HeI} = \begin{cases} \dfrac{b_9 M^{b_{10}}}{1+\alpha_1 \exp 15(M-M_{\rm HeF})} & M < M_{\rm HeF} \\ \dfrac{b_{11}+b_{12}M^{3.8}}{b_{13}+M^2} & M \geq M_{\rm HeF} \end{cases} \tag{49}$$

with $\alpha_1 = [b_9 M_{\rm HeF}^{b_{10}} - L_{\rm HeI}(M_{\rm HeF})]/L_{\rm HeI}(M_{\rm HeF})$. The radius at helium ignition is $R_{\rm HeI} = R_{\rm GB}(M, L_{\rm HeI})$ for $M \leq M_{\rm FGB}$, and $R_{\rm HeI} = R_{\rm mHe}$ for $M \geq \max(M_{\rm FGB}, 12.0)$, with $R_{\rm mHe}$ given by equation (55) below. If $M_{\rm FGB} < M < 12.0$, we take

$$R_{\rm HeI} = R_{\rm mHe}\left(\frac{R_{\rm GB}(L_{\rm HeI})}{R_{\rm mHe}}\right)^{\mu}, \quad \mu = \frac{\log(M/12.0)}{\log(M_{\rm FGB}/12.0)}. \tag{50}$$

The minimum luminosity during CHeB for IM stars, reached at the start of the blue phase, is given by

$$L_{\rm min,He} = L_{\rm HeI}\frac{b_{14}+cM^{b_{15}+0.1}}{b_{16}+M^{b_{15}}} \tag{51}$$

with

$$c = \frac{b_{17}}{M_{\rm FGB}^{0.1}} + \frac{b_{16}b_{17}-b_{14}}{M_{\rm FGB}^{b_{15}+0.1}},$$

so that $L_{\rm min,He} = b_{17}L_{\rm HeI}$ at $M = M_{\rm FGB}$. Continuity with HM stars, for which there is no minimum luminosity, is achieved by taking $b_{17} = 1$ for $Z \leq 0.002$ (but $b_{17} < 1$ for $Z > 0.002$). The radius at this point is $R_{\rm GB}(M, L_{\rm min,He})$.

For LM stars the ZAHB luminosity $L_{\rm ZAHB}$ takes the place of $L_{\rm min,He}$. To model the ZAHB continuously both with the minimum luminosity point at $M = M_{\rm HeF}$ and with the naked helium star ZAMS (see Section 6.1) for vanishing envelope mass ($M = M_{\rm c}$), the ZAHB position must depend on $M_{\rm c}$ as well as M. We define

$$\mu = \frac{M-M_{\rm c}}{M_{\rm HeF}-M_{\rm c}}, \tag{52}$$

so that $0 \leq \mu \leq 1$, and then take

$$\begin{aligned} L_{\rm ZAHB} &= L_{\rm ZHe}(M_{\rm c}) + \frac{1+b_{20}}{1+b_{20}\mu^{1.6479}} \\ &\quad \times \frac{b_{18}\mu^{b_{19}}}{1+\alpha_2 \exp 15(M-M_{\rm HeF})}, \\ \alpha_2 &= \frac{b_{18}+L_{\rm ZHe}(M_{\rm c})-L_{\rm min,He}(M_{\rm HeF})}{L_{\rm min,He}(M_{\rm HeF})-L_{\rm ZHe}(M_{\rm c})}, \end{aligned} \tag{53}$$

where $L_{\rm ZHe}$ is defined by equation (77). (Note that this α_2 is not a constant but depends on $M_{\rm c}$.) For the ZAHB radius we take

$$\begin{aligned} R_{\rm ZAHB} &= (1-f)R_{\rm ZHe}(M_{\rm c}) + fR_{\rm GB}(L_{\rm ZAHB}), \\ f &= \frac{(1.0+b_{21})\mu^{b_{22}}}{1.0+b_{21}\mu^{b_{23}}}. \end{aligned} \tag{54}$$

This formula ensures, apart from continuity at both ends, that $R_{\rm ZAHB}$ is always smaller than the GB radius at $L_{\rm ZAHB}$.

The minimum radius during the blue loop is approximated by

$$R_{\rm mHe} = \frac{b_{24}M + (b_{25}M)^{b_{26}}M^{b_{28}}}{b_{27}+M^{b_{28}}} \qquad M \geq M_{\rm HeF}. \tag{55}$$

Then for $M < M_{\rm HeF}$, we simply take

$$R_{\rm mHe} = R_{\rm GB}(L_{\rm ZAHB})\left\{\frac{R_{\rm mHe}(M_{\rm HeF})}{R_{\rm GB}[L_{\rm ZAHB}(M_{\rm HeF})]}\right\}^{\mu}$$

to keep $R_{\rm mHe}$ continuous, where $\mu = M/M_{\rm HeF}$.

The luminosity at the base of the AGB (or the end of CHeB) is given by

$$L_{\rm BAGB} = \begin{cases} \dfrac{b_{29}M^{b_{30}}}{1+\alpha_3 \exp 15(M-M_{\rm HeF})} & M < M_{\rm HeF} \\ \dfrac{b_{31}+b_{32}M^{b_{33}+1.8}}{b_{34}+M^{b_{33}}} & M \geq M_{\rm HeF} \end{cases} \tag{56}$$

with $\alpha_3 = [b_{29}M_{\rm HeF}^{b_{30}} - L_{\rm BAGB}(M_{\rm HeF})]/L_{\rm BAGB}(M_{\rm HeF})$. The radius at the BAGB is simply $R_{\rm AGB}(M, L_{\rm BAGB})$, as given by equation (74).

The lifetime of CHeB is given by

$$t_{\rm He} = \begin{cases} \{b_{39}+[t_{\rm HeMS}(M_{\rm c})-b_{39}](1-\mu)^{b_{40}}\} \\ \quad \times[1+\alpha_4 \exp 15(M-M_{\rm HeF})] & M < M_{\rm HeF} \\ t_{\rm BGB}\dfrac{b_{41}M^{b_{42}}+b_{43}M^5}{b_{44}+M^5} & M \geq M_{\rm HeF} \end{cases} \tag{57}$$

with $\alpha_4 = [t_{\rm He}(M_{\rm HeF}) - b_{39}]/b_{39}$. The term involving $t_{\rm HeMS}(M_{\rm c})$ ensures continuity with the lifetime of a naked helium star with $M = M_{\rm c}$ as the envelope mass vanishes. The lifetime of the blue phase of CHeB relative to $t_{\rm He}$ depends in a complicated way on M and Z; it is roughly approximated by

$$\tau_{\rm bl} = \begin{cases} 1 & M < M_{\rm HeF} \\ b_{45}\left(\dfrac{M}{M_{\rm FGB}}\right)^{0.414} + \alpha_{\rm bl}\left(\log\dfrac{M}{M_{\rm FGB}}\right)^{b_{46}} & \\ & M_{\rm HeF} \leq M \leq M_{\rm FGB} \\ (1-b_{47})\dfrac{f_{\rm bl}(M)}{f_{\rm bl}(M_{\rm FGB})} & M > M_{\rm FGB}, \end{cases} \tag{58}$$

truncated if necessary to give $0 \leq \tau_{\rm bl} \leq 1$, where

$$\alpha_{\rm bl} = \left[1-b_{45}\left(\frac{M_{\rm HeF}}{M_{\rm FGB}}\right)^{0.414}\right]\left(\log\frac{M_{\rm HeF}}{M_{\rm FGB}}\right)^{-b_{46}}$$

and

$$f_{\rm bl}(M) = M^{b_{48}}\left\{1-\frac{R_{\rm mHe}(M)}{R_{\rm AGB}[L_{\rm HeI}(M)]}\right\}^{b_{49}}.$$

The second term in the IM part of equation (58), with $\alpha_{\rm bl}$ as defined, ensures that $\tau_{\rm bl} = 1$ at $M = M_{\rm HeF}$. By taking $b_{45} = 1$ for $Z \leq 0.002$, we also have $\tau_{\rm bl} = 1$ at $M = M_{\rm FGB}$. The HM part also yields $\tau_{\rm bl} = 1$ at $M = M_{\rm FGB}$ for $Z \leq 0.002$, so that the transition is continuous for low Z. For $Z > 0.002$ the transition is regretably discontinuous. Finally, the radius dependence of $f_{\rm bl}$ ensures that $\tau_{\rm bl} = 0$ at the same mass where $R_{\rm mHe} = R_{\rm AGB}(L_{\rm HeI})$, i.e., where the blue phase vanishes.

During CHeB, we use the relative age $\tau = (t - t_{\rm HeI})/t_{\rm He}$, which takes values between 0 and 1. We define τ_x as the relative age at the start of the blue phase of CHeB, and L_x and R_x are the luminosity and radius at this epoch. Hence $\tau_x = 0$ for both the LM and HM regime, and $\tau_x = 1 - \tau_{\rm bl}$ for IM stars,

$$L_x = \begin{cases} L_{\rm ZAHB} & M < M_{\rm HeF} \\ L_{\rm min,He} & M_{\rm HeF} \leq M < M_{\rm FGB} \\ L_{\rm HeI} & M \geq M_{\rm FGB} \end{cases} \tag{59}$$

and

$$R_x = \begin{cases} R_{\rm ZAHB} & M < M_{\rm HeF} \\ R_{\rm GB}(L_{\rm min,He}) & M_{\rm HeF} \le M < M_{\rm FGB} \\ R_{\rm HeI} & M \ge M_{\rm FGB} \end{cases}. \quad (60)$$

Then the luminosity during CHeB is modelled as

$$L = \begin{cases} L_x \left(\dfrac{L_{\rm BAGB}}{L_x} \right)^{\lambda} & \tau_x \le \tau \le 1 \\ L_x \left(\dfrac{L_{\rm HeI}}{L_x} \right)^{\lambda'} & 0 \le \tau < \tau_x \end{cases} \quad (61)$$

where

$$\lambda = \left(\frac{\tau - \tau_x}{1 - \tau_x} \right)^{\xi}; \quad \xi = \min[2.5, \max(0.4, R_{\rm mHe}/R_x)], \quad (62)$$

$$\lambda' = \left(\frac{\tau_x - \tau}{\tau_x} \right)^3. \quad (63)$$

The *actual* minimum radius during CHeB is $R_{\rm min} = \min(R_{\rm mHe}, R_x)$, because equation (55) for $R_{\rm mHe}$ can give a value that is greater than R_x (this property is used, however, to compute ξ above). Furthermore, we define τ_y as the relative age at the end of the blue phase of CHeB, and L_y and R_y as the luminosity and radius at $\tau = \tau_y$. Hence $\tau_y = 1$ for LM and IM stars, and $\tau_y = \tau_{\rm bl}$ for HM stars. L_y is given by equation (61) ($L_y = L_{\rm BAGB}$ for $M \le M_{\rm FGB}$), and $R_y = R_{\rm AGB}(L_y)$. The radius during CHeB is modelled as

$$R = \begin{cases} R_{\rm GB}(M, L) & 0 \le \tau < \tau_x \\ R_{\rm AGB}(M, L) & \tau_y < \tau \le 1 \\ R_{\rm min} \exp(|\rho|^3) & \tau_x \le \tau \le \tau_y, \end{cases} \quad (64)$$

where

$$\rho = \left(\ln \frac{R_y}{R_{\rm min}} \right)^{\frac{1}{3}} \left(\frac{\tau - \tau_x}{\tau_y - \tau_x} \right) - \left(\ln \frac{R_x}{R_{\rm min}} \right)^{\frac{1}{3}} \left(\frac{\tau_y - \tau}{\tau_y - \tau_x} \right). \quad (65)$$

The core mass $M_{\rm c,HeI}$ at helium ignition is given by the $M_{\rm c}$–L relation for LM stars, while for $M \ge M_{\rm HeF}$ the same formula can be used as for the BGB core mass (equation 44), replacing $M_{\rm c}[L_{\rm BGB}(M_{\rm HeF})]$ with $M_{\rm c}[L_{\rm HeI}(M_{\rm HeF})]$ to ensure continuous transition at $M = M_{\rm HeF}$. For $M > 3\,{\rm M}_\odot$, $M_{\rm c,HeI}$ is nearly equal to $M_{\rm c,BGB}$. The core mass at the BAGB point is approximated by

$$M_{\rm c,BAGB} = (b_{36} M^{b_{37}} + b_{38})^{\frac{1}{4}}, \quad (66)$$

where $b_{36} \approx 4.36 \times 10^{-4}$, $b_{37} \approx 5.22$ and $b_{38} \approx 6.84 \times 10^{-2}$. In between, the core mass is taken to simply increase linearly with time:

$$M_{\rm c} = (1 - \tau) M_{\rm c,HeI} + \tau M_{\rm c,BAGB}. \quad (67)$$

5.4 Asymptotic giant branch

During the EAGB, when the hydrogen-burning shell is extinct, the (hydrogen-exhausted) core mass $M_{\rm c,He}$ (which we have been calling $M_{\rm c}$ so far, because it was the only significant core) stays constant at the value $M_{\rm c,BAGB}$. Within the hydrogen-exhausted core a degenerate carbon-oxygen core, $M_{\rm c,CO}$, has formed and begins to grow. At a time corresponding to the second dredge-up phase the growing $M_{\rm c,CO}$ catches the hydrogen-exhausted core, and the TPAGB begins. From then on, $M_{\rm c,CO}$ and $M_{\rm c,He}$ are equal and grow at the same rate (we neglect the mass, about $0.01\,{\rm M}_\odot$, of the thin helium layer between the two burning shells).

So on the EAGB we set

$$M_{\rm c} = M_{\rm c,He} = M_{\rm c,BAGB}.$$

Inside this core, $M_{\rm c,CO}$ grows by He-shell burning, at a rate dictated by the $M_{\rm c}$–L relation. Thus we can compute the evolution of $M_{\rm c,CO}$ and L in the same way as was done for GB stars using equations (37) and (39) with $M_{\rm c}$ replaced by $M_{\rm c,CO}$, $t_{\rm BGB}$ replaced by $t_{\rm BAGB}$ ($= t_{\rm HeI} + t_{\rm He}$) and $L_{\rm BGB}$ replaced by $L_{\rm BAGB}$. We also need to replace $A_{\rm H}$ with the value appropriate for helium burning, $A_{\rm He}$. The detailed models (Pols et al. 1998) on the EAGB show that the carbon-oxygen core is composed of 20 per cent carbon and 80 per cent oxygen by mass, so for every four carbon atoms produced by the triple-α reaction, three will capture an α particle and be converted to oxygen. Thus

$$E = \frac{\epsilon_{3\alpha} + 0.75\epsilon_{C\alpha}}{15 m(H)} \approx 8.09 \times 10^{17}\ {\rm erg\,g^{-1}},$$

so that

$$A_{\rm He} = (E X_{\rm He})^{-1} = 7.66 \times 10^{-5}\ {\rm M_\odot\,L_\odot^{-1}\,Myr^{-1}} \quad (68)$$

using $X_{\rm He} \approx 0.98$. Although massive stars ($M \gtrsim 8$) do not actually follow a $M_{\rm c}$–L relation for the CO core, by making the proper (ad hoc) assumptions about the constants in the relation, we can still effectively model their evolution in the same way as for true AGB stars.

As already mentioned, the EAGB ends when the the growing CO core reaches the hydrogen-exhausted core. If $0.8 < M_{\rm c,BAGB} < 2.25$, the star will undergo a second dredge-up phase at the end of the EAGB phase. During this second dredge-up the core mass is reduced to

$$M_{\rm c,DU} = 0.44 M_{\rm c,BAGB} + 0.448.$$

We assume that the second dredge-up takes place instantaneously at the moment when $M_{\rm c,CO}$ reaches the value $M_{\rm c,DU}$, so that also $M_{\rm c,CO} = M_{\rm c}$ at that point (but note that there is then a sudden discontinuity in $M_{\rm c} = M_{\rm c,He}$). Similarly, for $M_{\rm c,BAGB} \le 0.8$, the EAGB ends when $M_{\rm c,CO}$ reaches $M_{\rm c,He}$ without a second dredge-up, i.e., $M_{\rm c,DU} = M_{\rm c,BAGB}$. Stars with $M_{\rm c,BAGB} > 2.25$ do not undergo second dredge-up, as they can ignite carbon non-degenerately, and their evolution terminates before they ever reach the TPAGB.

To determine when the transition from EAGB to TPAGB occurs, we can simply insert $M_{\rm c,DU}$ into the $M_{\rm c}$–L relation to find $L_{\rm DU}$. Then we calculate

$$t_{\rm DU} = \begin{cases} t_{\rm inf,1} - \dfrac{1}{(p-1)A_{\rm He}D} \left(\dfrac{D}{L_{\rm DU}} \right)^{\frac{p-1}{p}} & L_{\rm DU} \le L_x \\ t_{\rm inf,2} - \dfrac{1}{(q-1)A_{\rm He}B} \left(\dfrac{B}{L_{\rm DU}} \right)^{\frac{q-1}{q}} & L_{\rm DU} > L_x \end{cases}. \quad (70)$$

Thus if $t > t_{\rm DU}$, the TPAGB has begun and the hydrogen-exhausted and helium-exhausted cores grow together as a common core. Once again the $M_{\rm c}$–L relation is obeyed, and once again we can use it in the same way as we did for GB stars if we replace $t_{\rm BGB}$ by $t_{\rm DU}$ and $L_{\rm BGB}$ by $L_{\rm DU}$. As we have both hydrogen and helium shell burning in operation, we must also replace $A_{\rm H}$ by an effective combined rate $A_{\rm H,He}$, where

$$A_{\rm H,He} = \frac{A_{\rm H} A_{\rm He}}{A_{\rm H} + A_{\rm He}} \simeq 1.27 \times 10^{-5}\ {\rm M_\odot\,L_\odot^{-1}\,Myr^{-1}}. \quad (71)$$

There is, however, an added complication that it is possible for $L_{\rm DU} > L_x$. In this case, $t_{\rm inf,1}$ and t_x are not needed, and $t_{\rm inf,2}$ is given by

$$t_{\rm inf,2} = t_{\rm DU} + \frac{1}{(q-1)A_{\rm H,He}B}\left(\frac{B}{L_{\rm DU}}\right)^{\frac{q-1}{q}}. \quad (72)$$

In this way the L evolution (and thus the R evolution) remains continuous through the second dredge-up.

On the TPAGB we do not model the thermal pulses individually, but we do take into account the most important effect of the thermally pulsing behaviour on the long-term evolution, namely that of third dredge-ups. During each interpulse period, the helium core grows steadily, but during the thermal pulse itself the convective envelope reaches inwards and takes back part of the mass previously eaten up by the core. The fraction of this mass is denoted by λ. Frost (1997) shows that models with $4 \leq M \leq 6$ and $0.004 \leq Z \leq 0.02$ have similar overall behaviour in λ, where λ increases quickly and reaches approximately 0.9 after about 5 pulses at which it stays nearly constant for the remaining pulses. For lower mass stars there is no evidence for such a high λ, with a value of 0.3 more likely for models of approximately solar mass, and then a steady increase of λ with M to reach $\lambda_{\rm max} \approx 0.9$ before $M = 4$ (Lattanzio 1989; Karakas et al., in preparation) Thus we simply take λ as constant for each M without any Z-dependence,

$$\lambda = \min(0.9, 0.3 + 0.001M^5). \quad (73)$$

Hence the secular growth of the core mass is reduced with respect to that given by the $M_{\rm c}$–L relation by a fraction λ. On the other hand, detailed calculations show that the luminosity evolution with time follows the same relation as without third dredge-up (Frost 1997), i.e., it keeps following equations (37) and (39) as if $M_{\rm c}$ were not reduced by dredge-up. In other words, the $M_{\rm c}$–L relation is no longer satisfied in the presence of third dredge-up, but we can use it nevertheless to compute the evolution of L, while $M_{\rm c}$ is modified as follows:

$$M_{\rm c} = M_{\rm c,DU} + (1-\lambda)(M'_{\rm c} - M_{\rm c,DU}),$$

where $M'_{\rm c}$ is from the $M_{\rm c}$–L relationship, with no dredge-up, and $M_{\rm c,DU}$ is the value of $M_{\rm c}$ at the start of the TPAGB.

The radius evolution is very similar to that of the GB, as the stars still have a deep convective envelope, but with some slight modifications. The basic formula is the same,

$$R_{\rm AGB} = A(L^{b_1} + b_2 L^{b_{50}}). \quad (74)$$

where indeed b_1 and b_2 are exactly the same as for $R_{\rm GB}$, and $b_{50} = b_{55}b_3$ for $M \geq M_{\rm HeF}$. Also, for $M \geq M_{\rm HeF}$,

$$A = \min(b_{51}M^{-b_{52}}, b_{53}M^{-b_{54}}),$$

which gives

$$R_{\rm AGB} = 1.125M^{-0.33}(L^{0.4} + 0.383L^{0.76}),$$

as an example, for $Z = 0.02$. For $M < M_{\rm HeF}$ the behaviour is slightly altered, so we take

$$b_{50} = b_3$$

$$A = b_{56} + b_{57}M$$

for $M \leq M_{\rm HeF} - 0.2$ and linear interpolation between the bounding values for $M_{\rm HeF} - 0.2 < M < M_{\rm HeF}$, which means that for $M = 1.0$ and $Z = 0.02$ the relation gives

$$R_{\rm AGB} \approx 0.95(L^{0.4} + 0.383L^{0.74}).$$

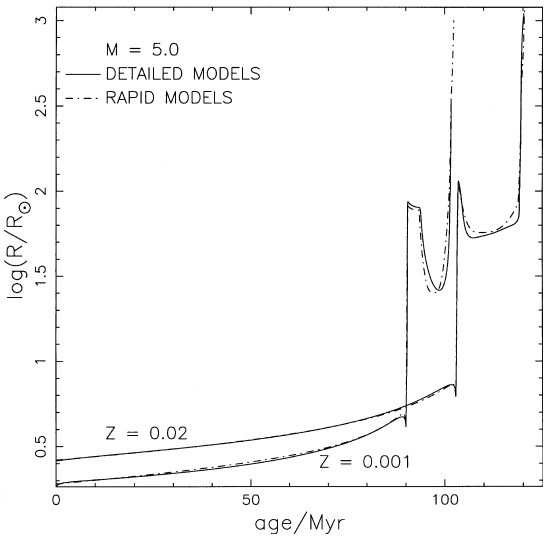

Figure 13. Radius evolution from the ZAMS to the end of the AGB for a 5.0-$M_\odot$ star, for metallicities 0.001 and 0.02, showing the detailed model points (solid lines) and the fitted tracks (dot-dashed lines).

In Fig. 13 we show the radius evolution of a 5.0-$M_\odot$ star, for $Z = 0.001$ and 0.02, from the ZAMS to the end of the AGB, from both the rapid evolution formulae and the detailed models. The AGB phase of the evolution is recognized by the sharp increase in radius following the phase of decreasing radius during the CHeB blue loop. An accurate fit to the AGB radius is required if the formulae are to be used in conjunction with binary evolution where factors such as Roche-lobe overflow and tidal circularization come into play. In fact, Fig. 13 shows that we achieve an accurate fit for all phases of the evolution.

We have now described formulae which cover all phases of the evolution covered by the detailed grid of stellar models. Figs 14 and 15 show synthetic HRDs derived from the formulae and are designed to be direct comparisons to Figs 1 and 2, respectively. The excellent performance of the fitting formulae is clearly evident.

6 FINAL STAGES AND REMNANTS

The AGB evolution is terminated, if not by complete loss of the envelope, when the CO-core mass reaches a maximum value given by

$$M_{\rm c,SN} = \max(M_{\rm Ch}, 0.773M_{\rm c,BAGB} - 0.35). \quad (75)$$

When this maximum core mass is reached before the envelope is lost, a *supernova* explosion is assumed to take place. For stars with $M_{\rm c,BAGB} \leq 2.25$, this should occur during the TPAGB phase. In practice, mass-loss will prevent it from doing so in most cases of single star evolution, but it may occur as a consequence of binary evolution. For such stars, we make a further distinction based on whether $M_{\rm c,BAGB}$ exceeds $1.6\,{\rm M}_\odot$. For $M_{\rm c,BAGB} < 1.6$, when the CO-core mass reaches $M_{\rm Ch}$ carbon ignites in a degenerate flash, leading to a thermonuclear explosion. It is uncertain whether we should expect this to occur for normal SSE, but if it does, then the supernova would be something like 'type IIa' (Ia + hydrogen), and we assume that such a supernova leaves no stellar remnant.

For $1.6 \leq M_{\rm c,BAGB} \leq 2.25$, the detailed models show that carbon ignites off-centre under semidegenerate conditions when

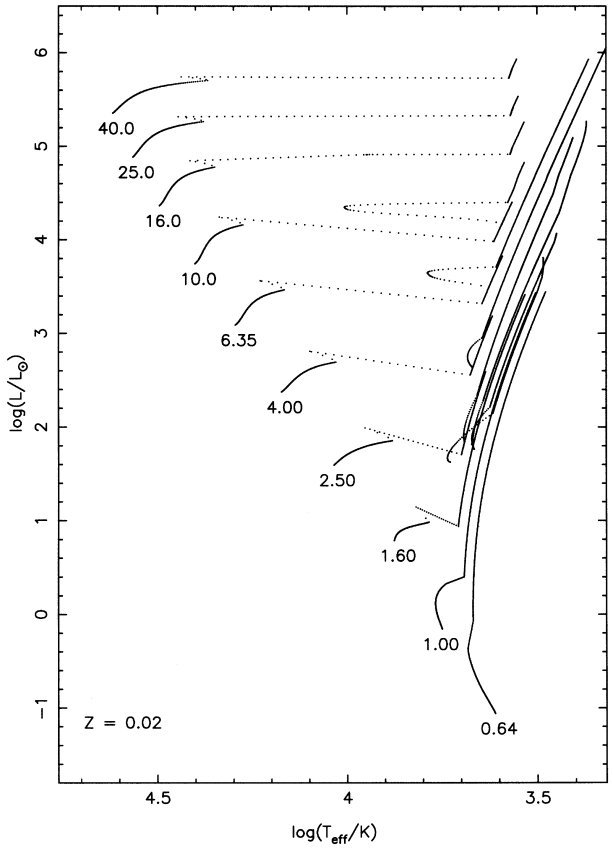

Figure 14. Same as Fig. 1, but tracks are from the evolution formulae.

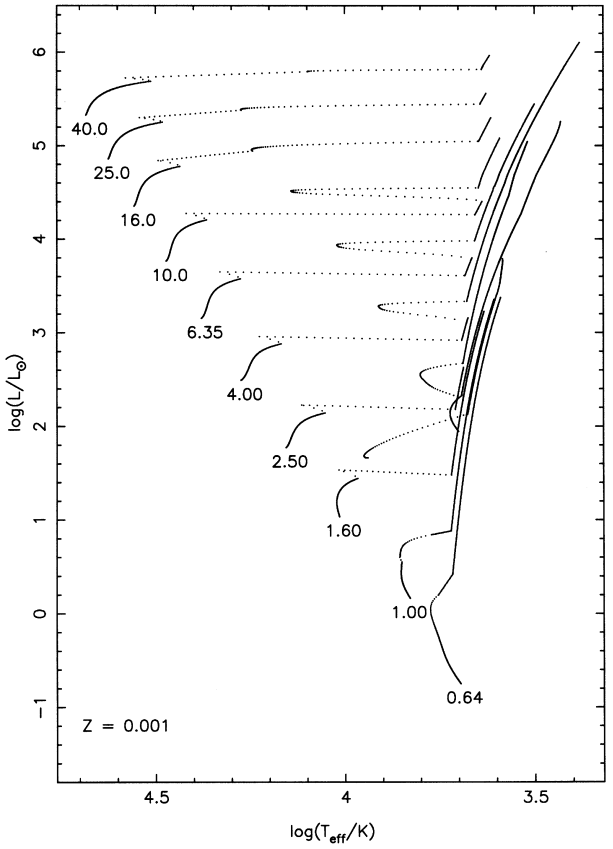

Figure 15. Same as Fig. 2, but tracks are from the evolution formulae.

$M_{\rm c,CO} \gtrsim 1.08$ (Pols et al. 1998). Carbon burning is expected to lead to the formation of a degenerate ONe core (Nomoto 1984), while the star continues its evolution up the AGB. When the core mass reaches $M_{\rm Ch}$, the ONe core collapses owing to electron capture on Mg^{24} nuclei. The resulting supernova explosion leaves a neutron star remnant (Section 6.2.2). The limiting $M_{\rm c,BAGB}$ values of 1.6 and 2.25 $M_\odot$ correspond to initial stellar masses denoted traditionally by the symbols $M_{\rm up}$ and $M_{\rm ec}$, respectively. The values of $M_{\rm up}$ and $M_{\rm ec}$ depend on metallicity (see table 1 of Pols et al. 1998), this dependence follows from inverting equation (66) for the values $M_{\rm c,BAGB} = 1.6$ and 2.25, respectively.

If the envelope is lost before $M_{\rm c}$ reaches $M_{\rm c,SN}$ ($= M_{\rm Ch}$) on the TPAGB, the remnant core becomes a white dwarf. This will be the case for almost all cases of normal SSE. For $M_{\rm c,BAGB} < 1.6$, this will be a CO white dwarf; for $M_{\rm c,BAGB} \geq 1.6$, it will be a ONe white dwarf (Section 6.2.1).

Stars with $M_{\rm c,BAGB} > 2.25$ develop non-degenerate CO cores which grow only slightly before undergoing central carbon burning, rapidly followed by burning of heavier elements. Here, $M_{\rm c,SN}$ is the CO-core mass at which this burning takes place, because the core mass does not grow significantly after carbon burning. Very quickly, an Fe-core is formed which collapses owing to photodisintegration, resulting in a supernova explosion. The supernova leaves either a neutron star or, for very massive stars, a black hole (Section 6.2.2). We assume that a black hole forms if $M_{\rm c,SN} > 7.0$, corresponding to $M_{\rm c,BAGB} > 9.52$.

This means that the lowest mass star to produce a NS has an initial mass M_* in the range $M_{\rm up} \leq M_* \leq M_{\rm ec}$, with the actual value of M_* depending greatly on the mass-loss rate. Observations would tend to suggest that $M_* \approx M_{\rm ec}$ (Elson et al. 1998), and indeed we find that with our adopted mass-loss rate (Section 7.1) almost all cases of SSE result in WD formation for $M \leq M_{\rm ec}$.

While most stars have their nuclear burning evolution terminated on the TPAGB, we must make allowances for cases of enhanced mass-loss, e.g., owing to binary evolution processes, that result in termination at an earlier nuclear burning stage. If the star loses its envelope during the HG or GB phases, then it will become either a HeWD (Section 6.2.1), if it has a degenerate core ($M < M_{\rm HeF}$), or a zero-age naked helium star (Section 6.1). If during CHeB $M = M_{\rm c}$, then an evolved naked helium star is formed with the degree of evolution determined by the amount of central helium already burnt. Thus the age of the new star is taken to be

$$t = \left(\frac{t' - t'_{\rm HeI}}{t'_{\rm He}} \right) t_{\rm HeMS}, \tag{76}$$

where the primes denote times for the original star, and $t_{\rm HeMS}$ is given by equation (79). When the envelope is lost during the EAGB so that $M_{\rm c,He} = M$, a naked helium giant (Section 6.1) is formed as unburnt helium still remains within $M_{\rm c,He}$ through which the growing $M_{\rm c,CO}$ is eating. The age of the new star will be fixed by using $M_{\rm c} = M_{\rm c,CO}$ and $M = M_{\rm c,He}$ in the HeGB $M_{\rm c}$–t relation (see Section 6.1). We note that although naked helium stars are nuclear burning stars, i.e., not a final state, we still label them as a remnant stage because they are the result of mass-loss. Also, when a WD, NS or BH is formed, the age of the star is reset so that the remnant begins its evolution at zero-age to allow for cooling (Section 6.2).

6.1 Naked helium stars

The formulae described in this section are based on detailed stellar evolution models for naked helium stars, computed by one of the authors (ORP) with the same code as used for the stellar models described in Section 3. First, a helium ZAMS of homogeneous models in thermal equilibrium was constructed, with composition $X = 0$, $Y = 0.98$ and $Z = 0.02$. Starting from this ZAMS, evolution tracks were computed for masses between 0.32 and $10\,\mathrm{M}_\odot$, spaced by approximately 0.1 in $\log M$. For masses below $2\,\mathrm{M}_\odot$, the tracks were computed until the end of shell helium burning, and for $M > 2\,\mathrm{M}_\odot$, up to or through central carbon burning. These models will be discussed in more detail in a forthcoming paper (Pols, in preparation).

The following analytic formulae provide an accurate fit to the ZAMS luminosity and radius of naked helium stars with $Z = 0.02$:

$$L_{\mathrm{ZHe}} = \frac{15\,262M^{10.25}}{M^9 + 29.54M^{7.5} + 31.18M^6 + 0.0469}, \tag{77}$$

$$R_{\mathrm{ZHe}} = \frac{0.2391M^{4.6}}{M^4 + 0.162M^3 + 0.0065}. \tag{78}$$

The central helium-burning lifetime (helium MS) is approximated by

$$t_{\mathrm{HeMS}} = \frac{0.4129 + 18.81M^4 + 1.853M^6}{M^{6.5}}. \tag{79}$$

The behaviour of L and R during central helium burning can be approximated by

$$L_{\mathrm{HeMS}} = L_{\mathrm{ZHe}}(1 + 0.45\tau + \alpha\tau^2) \tag{80}$$

and

$$R_{\mathrm{HeMS}} = R_{\mathrm{ZHe}}(1 + \beta\tau - \beta\tau^6), \tag{81}$$

where $\tau = t/t_{\mathrm{HeMS}}$, and t is counted from the He ZAMS. α and β are dependent on mass, as follows:

$$\alpha = \max(0, 0.85 - 0.08M) \tag{82}$$

and

$$\beta = \max(0, 0.4 - 0.22\log M). \tag{83}$$

The evolution after the helium MS is dominated by the growth of the degenerate C-O core for low-mass stars, and by evolution up to carbon burning for $M \gtrsim 2$. Low-mass helium stars follow an approximate core mass–luminosity relation (e.g. Jeffery 1988), and we compute their evolution making use of this relation just as we do for GB stars (Section 5.2). For massive helium stars, although they do not properly follow such a relation, an ad hoc M_{c}–L relation can be used to also describe their evolution. The following formula works for the whole mass range:

$$L_{\mathrm{HeGB}} = \min(BM_{\mathrm{c}}^3, DM_{\mathrm{c}}^5), \tag{84}$$

with $B = 4.1 \times 10^4$ and $D = 5.5 \times 10^4/(1 + 0.4M^4)$. The first term models the 'real' M_{c}–L relation followed by low-mass helium stars, while the second, mass-dependent term mimics the behaviour for high-mass stars. The evolution of L and M_{c} with time is obtained from equation (84) and the equivalents of Equations (39)–(42), with A_{H} replaced by A_{He} as given by equation (68), t_{BGB} replaced by t_{HeMS}, and L_{BGB} replaced by L_{THe}. L_{THe} is the value of L at the end of the helium MS, i.e., L_{HeMS} given by equation (80) at $\tau = 1$. The post-HeMS radius can be approximated by

$$R_{\mathrm{HeGB}} = \min(R_1, R_2), \tag{85}$$

$$R_1 = R_{\mathrm{ZHe}}\left(\frac{L}{L_{\mathrm{THe}}}\right)^{0.2} + 0.02\left[\exp\left(\frac{L}{\lambda}\right) - \exp\left(\frac{L_{\mathrm{THe}}}{\lambda}\right)\right], \tag{86}$$

$$\lambda = 500\frac{2 + M^5}{M^{2.5}}, \tag{87}$$

$$R_2 = 0.08L^{0.75}. \tag{88}$$

The first term of R_1 models the modest increase in radius at low mass and/or L, and the second term the very rapid expansion and redward movement in the HRD for $M \gtrsim 0.8$ once L is large enough. The star is on what we call the naked helium HG (HeHG) if the radius is given by R_1. The radius R_2 mimics the Hayashi track for helium stars on the giant branch (HeGB). We make the distinction between HeHG and HeGB stars only because the latter have deep convective envelopes and will therefore respond differently to mass-loss.

The final stages of evolution are equivalent to those of normal stars, i.e., as discussed in Section 6, but with $M_{\mathrm{c,BAGB}}$ replaced by the helium-star initial mass M in equation (75) as well as in the discussion that follows it. If $M < 0.7\,\mathrm{M}_\odot$, the detailed models show that shell helium burning stops before the whole envelope is converted into C and O. We mimic this by letting a helium star become a CO WD when its core mass reaches the value

$$M_{\mathrm{c,max}} = \min(1.45M - 0.31, M), \tag{89}$$

as long as $M_{\mathrm{c,max}} < M_{\mathrm{c,SN}}$.

6.2 Stellar remnants

6.2.1 *White dwarfs*

We distinguish between three types of white dwarf, namely those composed of He (formed by complete envelope loss of a GB star with $M < M_{\mathrm{HeF}}$, expected only in binaries), those composed of C and O (formed by envelope loss of a TPAGB star with $M < M_{\mathrm{up}}$, see above), and those composed mainly of O and Ne (envelope loss of a TPAGB star with $M_{\mathrm{up}} \leq M \leq M_{\mathrm{ec}}$). The only distinction we make between CO and ONe white dwarfs is in the way they react to mass accretion. If $M_{\mathrm{WD}} + M_{\mathrm{acc}} > M_{\mathrm{Ch}}$, after accreting an amount of mass M_{acc}, then a CO WD explodes without leaving a remnant, while an ONe WD leaves a neutron star remnant with mass $M_{\mathrm{NS}} = 1.17 + 0.09(M_{\mathrm{WD}} + M_{\mathrm{acc}})$ (see later in Section 6.2.2). The Chandrasekhar mass is given by

$$M_{\mathrm{Ch}} \approx \left(\frac{5.8}{\mu_{\mathrm{e}}^2}\right)\mathrm{M}_\odot,$$

so it is composition-dependent, but the mean molecular weight per electron is $\mu_{\mathrm{e}} \approx 2$, except for low-mass MS stars in cataclysmic variables, so we use $M_{\mathrm{Ch}} = 1.44$ at all times.

The luminosity evolution of white dwarfs is modelled using standard cooling theory (Mestel 1952); see Shapiro & Teukolsky (1983, p. 85):

$$L_{\mathrm{WD}} = \frac{635MZ^{0.4}}{[A(t + 0.1)]^{1.4}}, \tag{90}$$

where t is the age since formation, and A is the effective baryon number for the WD composition. For He WDs we have $A = 4$, for CO WDs $A = 15$, and for ONe WDs $A = 17$. Equation (90) is

adequate for relatively old WDs. The addition of a constant in the factor $(t + 0.1)$ mimics the fact that the initial cooling is rather faster than given by Mestel theory, as well as ensuring that it does not start at infinite L, so that we effectively start the evolution at a cooling age of 10^5 yr. Note that the initial cooling of the WD is modelled by the small-envelope pertubation functions on the TPAGB (see Section 6.3).

The radius of a white dwarf is given by

$$R_{\rm WD} = \max\left[R_{\rm NS}, 0.0115\sqrt{\left(\frac{M_{\rm Ch}}{M_{\rm WD}}\right)^{2/3} - \left(\frac{M_{\rm WD}}{M_{\rm Ch}}\right)^{2/3}}\right] \tag{91}$$

as in Tout et al. (1997).

6.2.2 *Neutron stars and black holes*

When a neutron star or black hole is formed in one of the situations given above, we assume that its gravitational mass is given by

$$M_{\rm NS} = 1.17 + 0.09M_{\rm c,SN}, \tag{92}$$

where $M_{\rm c,SN}$ is the mass of the CO-core at the time of supernova explosion. With equation (75), this leads to a minimum NS mass of $1.3\,{\rm M}_\odot$, and the criterion for BH formation $M_{\rm c,SN} > 7.0$ gives a maximum NS mass and minimum BH mass of $1.8\,{\rm M}_\odot$.

The NS cooling curve is approximated by assuming that photon emission is the dominant energy loss mechanism, which should be true for $t \geq 10^6$ yr (see Shapiro & Teukolsky 1983, p. 330):

$$L_{\rm NS} = \frac{0.02M^{2/3}}{[\max(t, 0.1)]^2}. \tag{93}$$

The upper limit is calibrated to give $T_{\rm eff} \approx 2 \times 10^6\,{\rm K}$, which is appropriate for the Crab pulsar and is set constant for the first 10^5 yr to reflect the scatter in the observations of $T_{\rm eff}$ for pulsars with an age less than 10^5 yr. Equation (93) also ensures that $L_{\rm NS} < L_{\rm WD}$ at all times, and that neutron stars will cool faster than white dwarfs.

The radius of a NS is simply set to 10 km, i.e., $R_{\rm NS} = 1.4 \times 10^{-5}$.

We take the black hole radius as the Schwarzschild radius:

$$R_{\rm BH} = \frac{2GM_{\rm BH}}{c^2} = 4.24 \times 10^{-6}M_{\rm BH}. \tag{94}$$

The corresponding luminosity of a BH is approximately given by

$$L_{\rm BH} = \frac{1.6 \times 10^{-50}}{M_{\rm BH}^2} \tag{95}$$

(Carr & Hawking 1974), which will be negligible except for extremely low-mass objects, and thus we actually set

$$L_{\rm BH} = 10^{-10} \tag{96}$$

to avoid floating-point division by zero.

Note that for all remnants we set $M_{\rm c} = M$ for convenience.

6.3 Small-envelope behaviour and hot subdwarfs

In general, the equations in Section 5 accurately describe the nuclear burning evolution stages as outlined by our grid of detailed models. However, we also find it necessary to add some pertubation functions which alter the radius and luminosity when the envelope becomes small in mass, in order to achieve a smooth transition in the HRD towards the position of the remnant. Take, for example, the AGB radius where

$$R_{\rm AGB} \propto M^{-x},$$

so that as M decreases due to mass-loss from a stellar wind $R_{\rm AGB}$ will increase and the star moves further to the red in the HRD. In fact, as the envelope mass ($M_{\rm env}$) gets very small, the star becomes bluer and moves across the HRD to WD temperatures. In the same way we would also expect the luminosity growth rate to decrease until the luminosity levels off at some approximately constant value for small $M_{\rm env}$.

Thus for any nuclear burning evolution stage where there is a well-defined core and envelope (i.e., not the MS), we define

$$\mu = \left(\frac{M - M_{\rm c}}{M}\right)\min\left\{5.0, \max\left[1.2, \left(\frac{L}{L_0}\right)^\kappa\right]\right\}, \tag{97}$$

where $L_0 = 7.0 \times 10^4$, $\kappa = -0.5$ for normal giants, and

$$\mu = 5\left(\frac{M_{\rm c,max} - M_{\rm c}}{M_{\rm c,max}}\right) \tag{98}$$

for helium giants. Then, if $\mu < 1.0$, we perturb the luminosity and radius using

$$L' = L_{\rm c}\left(\frac{L}{L_{\rm c}}\right)^s \tag{99}$$

$$R' = R_{\rm c}\left(\frac{R}{R_{\rm c}}\right)^r, \tag{100}$$

where

$$s = \frac{(1 + b^3)(\mu/b)^3}{1 + (\mu/b)^3} \tag{101}$$

$$r = \frac{(1 + c^3)(\mu/c)^3\mu^{0.1/q}}{1 + (\mu/c)^3}, \tag{102}$$

with

$$b = 0.002\max\left(1, \frac{2.5}{M}\right) \tag{103}$$

$$c = 0.006\max\left(1, \frac{2.5}{M}\right) \tag{104}$$

$$q = \log_{\rm e}\left(\frac{R}{R_{\rm c}}\right). \tag{105}$$

The luminosity and radius of the star are then given by L' and R'.

In the above formulae, $L_{\rm c}$ and $R_{\rm c}$ are the luminosity and radius of the remnant that the star would become if it lost all of its envelope immediately. Thus we set $M = M_{\rm c}$ in the appropriate remnant formulae. If the star is on the HG or GB, then we have, for $M < M_{\rm HeF}$,

$$L_{\rm c} = L_{\rm ZHe}(M_{\rm c})$$

$$R_{\rm c} = R_{\rm ZHe}(M_{\rm c}),$$

otherwise

$$L_{\rm c} = L_{\rm WD}(M_{\rm c}),$$

i.e., equation (90) with $A = 4$ and $t = 0$,

$$R_{\rm c} = R_{\rm WD}(M_{\rm c}).$$

During CHeB the remnant will be an evolved helium MS star so

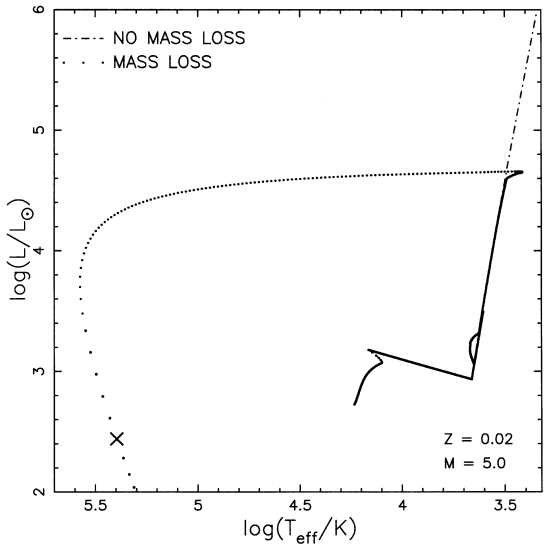

Figure 16. Synthetic evolution tracks on the HRD for a 5.0-$M_\odot$ star without mass-loss (dot-dashed line) and with mass-loss (points). The cross marks where the WD cooling track begins.

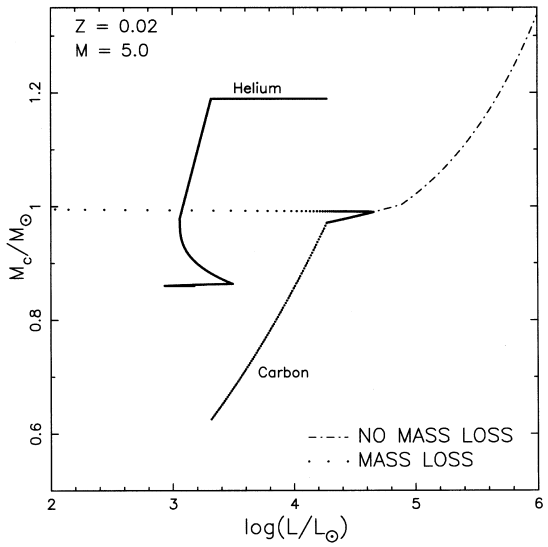

Figure 17. Relation between core mass and luminosity for a 5.0-$M_\odot$ star as given by the formulae without mass-loss (dot-dashed line) and with mass-loss (points). Both the helium and carbon-oxygen cores are shown for the EAGB phase.

we use M_c and $\tau = (t - t_{HeI})/t_{He}$ in equations (80) and (81) to give L_c and R_c, respectively. On the EAGB the remnant will be a helium HG or GB star with $M = M_{c,He}$, so that L_c comes from the HeGB M_c–L relation with $M_c = M_{c,CO}$ and R_c from $R_{HeGB} = (M_{c,He}, L_c)$. For the TPAGB, HeHG and HeGB the remnant will most likely be a CO WD, so

$$L_c = L_{WD}(M_c),$$

i.e., equation (90) with $A = 15$ and $t = 0$,

$$R_c = R_{WD}(M_c).$$

Fig. 16 shows how a model incorporating mass-loss (using the prescription outlined in Section 7.1) and the small-envelope pertubation functions deviates from a model without either. No difference is evident until the stellar wind becomes appreciable as the star evolves up the AGB. As the envelope mass is reduced, the star initially moves to the right of the AGB, becoming redder in accordance with equation (74). Then, as the envelope is reduced even further in mass, the star moves to the left in the HRD, under the influence of the pertubation functions, becoming bluer as the hot core starts to become visible. Thus we have in effect mimicked the planetary nebulae nucleus phase of evolution which finishes when the star joins up with the white dwarf cooling track (marked by a cross in the figure). The behaviour of the core mass–luminosity relation for the same models is shown in Fig. 17. Both the helium and the carbon-oxygen cores are shown on the AGB until second dredge-up when the helium core is reduced in mass and the two grow together. It can be seen that after second dredge-up the slope of the relation changes as a result of third dredge-up during the TPAGB phase.

We should note that R_c can be used directly as a fairly accurate estimate of the current core radius of the star except when R_c is given by R_{WD}. In that case, nuclear burning will be taking place in a thin shell separating the giant core from the envelope, so that the core will be a hot subdwarf for which we assume the radius $R_c \simeq 5R_{WD}(M_c)$. It is also necessary to check that $R_c \leq R$ in all cases.

7 MASS-LOSS AND ROTATION

7.1 Mass-loss

We now describe a particular mass-loss prescription which is independent of the previous formulae and fits observations well. On the GB and beyond, we apply mass-loss to the envelope according to the formula of Kudritzki & Reimers (1978),

$$\dot{M}_R = \eta 4 \times 10^{-13} \frac{\eta L R}{M} \, M_\odot \, yr^{-1}, \tag{106}$$

with a value of $\eta = 0.5$. Our value for η is within the limits set by observations of horizontal branch morphology in Galactic globular clusters (Iben & Renzini 1983), and we do not include a Z-dependence in equation (106) as there is no strong evidence that it is necessary (Iben & Renzini 1983; Carraro et al. 1996). On the AGB, we apply the formulation of Vassiliadis & Wood (1993),

$$\log \dot{M}_{VW} = -11.4 + 0.0125[P_0 - 100 \max(M - 2.5, 0.0)],$$

to give the observed rapid exponential increase in $\dot{M}$ with period before the onset of the the superwind phase. The steady superwind phase is then modelled by applying a maximum of $\dot{M}_{VW} = 1.36 \times 10^{-9} L \, M_\odot \, yr^{-1}$. P_0 is the Mira pulsation period given by

$$\log P_0 = \min(3.3, -2.07 - 0.9 \log M + 1.94 \log R).$$

For massive stars we model mass-loss over the entire HRD using the prescription given by Nieuwenhuijzen & de Jager (1990),

$$\dot{M}_{NJ} = 9.6 \times 10^{-15} \left(\frac{Z}{Z_\odot}\right)^{1/2} R^{0.81} L^{1.24} M^{0.16} \, M_\odot \, yr^{-1}$$

for $L > 4000 M_\odot$, modified by the factor $Z^{1/2}$ (Kudritzki et al. 1989).

For small hydrogen-envelope mass, $\mu < 1.0$, we also include a Wolf–Rayet-like mass-loss (Hamann, Koesterke & Wessolowski 1995; Hamann & Koesterke 1998), which we have reduced to give

$$\dot{M}_{WR} = 10^{-13} L^{1.5} (1.0 - \mu) \, M_\odot \, yr^{-1},$$

where μ is given by equation (97). The reduction is necessary in

order to produce sufficient black holes to match the number observed in binaries.

We then take the mass-loss rate as the dominant mechanism at that time:

$$\dot{M} = \max(\dot{M}_{\rm R}, \dot{M}_{\rm VW}, \dot{M}_{\rm NJ}, \dot{M}_{\rm WR})\,{\rm M}_\odot\,{\rm yr}^{-1}.$$

In addition, we add a LBV-like mass-loss for stars beyond the Humphreys–Davidson limit (Humphreys & Davidson 1994),

$$\dot{M}_{\rm LBV} = 0.1(10^{-5}RL^{1/2} - 1.0)^3\left(\frac{L}{6\times10^5} - 1.0\right){\rm M}_\odot\,{\rm yr}^{-1},$$

if $L > 6\times10^5$ and $10^{-5}RL^{1/2} > 1.0$, so that $\dot{M} = \dot{M} + \dot{M}_{\rm LBV}$.

For naked helium stars we include the Wolf–Rayet-like mass-loss rate to give

$$\dot{M} = \max[\dot{M}_{\rm R}, \dot{M}_{\rm WR}(\mu = 0)]\,{\rm M}_\odot\,{\rm yr}^{-1}.$$

The introduction of mass-loss means that we now have two mass variables, the initial mass M_0 and the current mass $M_t(= M)$. From tests with mass-loss on detailed evolution models we found that the luminosity and time-scales remain virtually unchanged when mass-loss is included, during the GB and beyond, but that the radius behaviour is very sensitive. Thus we use M_0 in all formulae that involve the calculation of time-scales, luminosity or core mass, and we use M_t in all radius formulae. When a MS star loses mass, which may occur in a stellar wind for massive stars or as a result of mass transfer, it will evolve down along the MS to lower L and $T_{\rm eff}$ because of the decrease in central density and temperature. The luminosity responds to changes in mass because the size of the core depends on the mass of the star, and therefore M_0, which is more correctly the effective initial mass, is kept equal to the current mass while the star is on the MS. We must effectively age the star, so that the fraction of MS lifetime remains unchanged, by using

$$t' = \frac{t'_{\rm MS}}{t_{\rm MS}}t,$$

where primes denote quantities after a small amount of mass-loss ($t'_{\rm MS} > t_{\rm MS}$, thus $t' > t$). Even though the star has been aged relative to stars of its new mass, its remaining MS lifetime has been increased. Naked helium MS stars must also be treated in the same way with $t_{\rm MS}$ replaced by $t_{\rm HeMS}$. During the giant phases of evolution the age determines the core mass which will be unaffected by mass changes at the surface, as the core and envelope are effectively decoupled in terms of the stellar structure, so that the age and the initial mass do not need to be altered. HG stars will respond to changes in mass on a thermal time-scale, and thus, as our detailed models show is necessary, we keep $M_0 = M_t$ during the HG, and the star is aged according to

$$t' = t'_{\rm MS} + \frac{(t'_{\rm BGB} - t'_{\rm MS})}{(t_{\rm BGB} - t_{\rm MS})}(t - t_{\rm MS})$$

whenever mass is lost. However, as the core mass depends on M_0, see Equations (28)–(30), there exists a limiting value beyond which M_0 cannot be decreased. To do otherwise would lead to an unphysical decrease in the core mass. Therefore our treatment of mass-loss on the HG is a mixture of the way the MS and giant phases are treated which in a sense reflects the transitional nature of the HG phase of evolution.

When a LM star experiences the helium flash and moves to the ZAHB we reset $M_0 = M_t$, so that $t = t_{\rm HeI}(M_0)$ as it is now a new star with no knowledge of its history. We also reset $M_0 = M_t$ when naked helium star evolution is begun.

7.1.1 *The white dwarf initial–final mass relation*

If a star is to evolve to become a WD, the minimum mass possible for the WD is the core mass at the start of the TPAGB. Thus an accurate empirical relation between WD masses and the initial mass of their progenitors provides an important calibration of the mass-loss required on the AGB. This helps to constrain η in equation (106) which, for now, is basically a free parameter. The commonly used method to obtain the initial–final mass relation (IFMR) for white dwarfs is to use WDs that are members of clusters with known ages. Their radii, masses and cooling times can be obtained spectroscopically so that by subtracting the cooling time from the cluster age the time spent by the progenitor from the ZAMS to the AGB can be estimated. The initial progenitor mass, $M_{\rm i}$, must then be derived using appropriate stellar models, so that this a semi-empirical method for defining the IFMR. Using data from WDs in Galactic open clusters, Weidemann (1987) derived such a semi-empirical IFMR as shown in Fig. 18. As Jeffries (1997) rightly points out, an IFMR derived by this method will be sensitive to the amount of core overshooting included in the stellar evolution models. The effect of increased overshooting is to decrease the derived cluster age, thus increasing the progenitor lifetime and decreasing $M_{\rm i}$. The IFMR will also be sensitive to changes in metallicity.

Jeffries (1997) presents initial and final masses for four WDs found in the young open cluster NGC 2516, which has a metallicity of $Z \simeq 0.009$. The initial progenitor masses are derived from the stellar models of Schaerer et al. (1993) with $Z = 0.008$ and moderate core overshooting. We show the data points for these four WDs in Fig. 18, as well as the IFMR given by our formulae for $Z = 0.02$ and 0.004 (the IFMR for $Z = 0.009$ will lie between these two), and the corresponding core mass at the start of the TPAGB. As the TPAGB core mass is the minimum possible mass for the WD, it is clear that our formulae are in disagreement with the semi-empirical IFMR of Weidemann

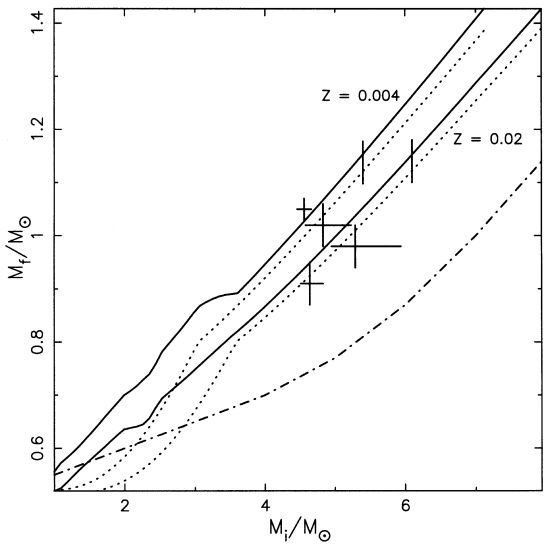

Figure 18. Relation between white dwarf mass and the ZAMS mass of its progenitor, i.e., the initial-final mass relation (IFMR). The IFMR from the evolution formulae (solid line) is given for $Z = 0.02$ and 0.004, as well as the corresponding core masses at the start of the TPAGB (dotted lines). The vertical lines correspond to $M_{\rm up}$. Weidemann's (1987) semi-empirical IFMR (dot-dashed line) and the NGC 2516 white dwarfs (crosses) from Jeffries (1997) are shown.

(1987). Jeffries (1997) was in similar disagreement with the semi-empirical IFMR. However, the IFMRs from our formulae are in good agreement with the NGC 2516 data, taking the associated errors of the data points into account. Thus there is no contradiction with the mass-loss prescription used for the formulae; however, we note that an empirical IFMR is required before concrete conclusions can be drawn.

7.2 Rotation

As we plan to use the evolution routines for single stars in binary star applications, it is desirable to follow the evolution of the stars' angular momentum. To do this, we must start each star with some realistic spin on the ZAMS. A reasonable fit to the $\bar{v}_{\rm rot}$ MS data of Lang (1992) is given by

$$\bar{v}_{\rm rot}(M) = \frac{330M^{3.3}}{15.0 + M^{3.45}}\ {\rm km\,s^{-1}}, \tag{107}$$

so that

$$\Omega = 45.35\frac{\bar{v}_{\rm rot}}{R_{\rm ZAMS}}\ {\rm yr^{-1}}. \tag{108}$$

The angular momentum is then given by

$$J_{\rm spin} = I\Omega = kMR^2\Omega,$$

where the constant k depends on the internal structure, e.g., $k = 2/5$ for a solid sphere and $k = 2/3$ for a spherical shell. In fact, we find the angular momentum by splitting the star into two parts, consisting of the core and the envelope, so that

$$J_{\rm spin} = [k_2(M - M_{\rm c})R^2 + k_3M_{\rm c}R_{\rm c}^2]\Omega, \tag{109}$$

where $k_2 = 0.1$, based on detailed giant models which reveal $k = 0.1M_{\rm env}/M$, and $k_3 = 0.21$ for an $n = 3/2$ polytrope such as a WD, NS or dense convective core. This works well for post-MS stars which have developed a dense core whose rotation is likely to have decoupled from the envelope, while also representing the near uniform rotation of homogenous MS stars which have $M_{\rm c} = 0.0$. When the star loses mass in a stellar wind, the wind will carry off angular momentum from the star at a rate given by

$$\dot{J} = k\dot{M}h,$$

where $h = R^2\Omega$. Thus

$$J_{\rm spin} = J_{\rm spin} - \tfrac{2}{3}\Delta MR^2\Omega \tag{110}$$

when the star loses an amount of mass ΔM, where we take $k = 2/3$, as we assume that all the mass is lost uniformly at the surface of the star, i.e., from a spherical shell.

We also include magnetic braking for stars that have appreciable convective envelopes where

$$\dot{J}_{\rm mb} = 5.83 \times 10^{-16}\frac{M_{\rm env}}{\rm M}(R\Omega)^3\,{\rm M_\odot\,R_\odot^2\,yr^{-2}}, \tag{111}$$

with Ω in units of years. However, following Rappaport, Verbunt & Joss (1983), we do not allow magnetic braking for fully convective stars, $M < 0.35$.

For most stars, $M_{\rm env}$ is simply given by $M - M_{\rm c}$; however, the case is slightly more complicated for MS and HG stars. Our detailed models show that MS stars are fully convective for $M < 0.35$ so that $M_{\rm env,0} = M$, and that MS stars with $M > 1.25$ have little or no convective envelope so that $M_{\rm env,0} = 0.0$, independent of Z. In between, we take

$$M_{\rm env,0} = 0.35\left(\frac{1.25 - M}{0.9}\right)^2 \quad 0.35 \le M \le 1.25.$$

The convective envelope, if it is present, will diminish as the star evolves across the MS, so we take

$$M_{\rm env} = M_{\rm env,0}(1.0 - \tau)^{1/4},$$

where

$$\tau = \frac{t}{t_{\rm MS}},$$

and $M_{\rm env,0}$ is effectively the ZAMS value. On the HG we assume that the convective core gradually establishes itself so that

$$M_{\rm env} = \tau(M - M_{\rm c}),$$

where

$$\tau = \frac{t - t_{\rm MS}}{t_{\rm BGB} - t_{\rm MS}}.$$

8 DISCUSSION

The possible paths of evolution through the various phases described in the preceeding sections are illustrated in Fig. 19. In Fig. 20 we show the distribution of remnant masses and types, as a function of initial stellar mass, for Population I and II stars as given by the rapid evolution code. The distribution approximates what we would see if a population of single stars were to be evolved to the current age of the Galaxy. The variation in behaviour produced by a change in metallicity should once again be noted. These variations are due to changes in the evolution rates as a function of initial mass, brought about by changes in the composition. The initial mass above which stars will become black holes rather than neutron stars is not well constrained, which is why we use the maximum AGB core mass in the formulae to decide the outcome, corresponding to a transition at $M_0 \simeq 30\,{\rm M_\odot}$ (varying with metallicity). It can also be seen from Fig. 20 that, above this mass, a small pocket of neutron star formation occurs in what would normally be assumed to be a region of black hole formation on the diagram. This behaviour corresponds to a massive star losing its envelope on the HG so that the star enters the naked helium MS phase, where the mass-loss rate increases, causing a reduction in M_0. As a result, a lower value than otherwise expected for $M_{\rm NS}$ is given by equation (92) when the naked helium evolution ends.

The formulae described in this paper are available in convenient subroutine form as a SSE package, which we also term 'the rapid evolution code', that contains:

(i) EVOLVE The main routine which, amongst other things, initializes the star, chooses the time-steps and implements mass-loss.

(ii) ZCNSTS Subroutine which sets all the constants of the formulae which depend on metallicity so that there is no Z-dependence elsewhere. This needs to be called each time Z is changed.

(iii) STAR Subroutine which derives the landmark time-scales and luminosities that divide the various evolution stages. It also calculates $t_{\rm N}$, which is an estimate of the end of the nuclear evolution, i.e., when $M_{\rm c} = \min(M_t, M_{\rm c,SN})$, assuming no further mass-loss.

(iv) HRDIAG Subroutine to decide which evolution stage the star is currently at, and then to calculate the appropriate L, R and $M_{\rm c}$.

(v) ZFUNCS Contains all the detailed evolution formulae as functions.

(vi) MLWIND derives the mass-loss as a function of evolution stage and the current stellar properties.

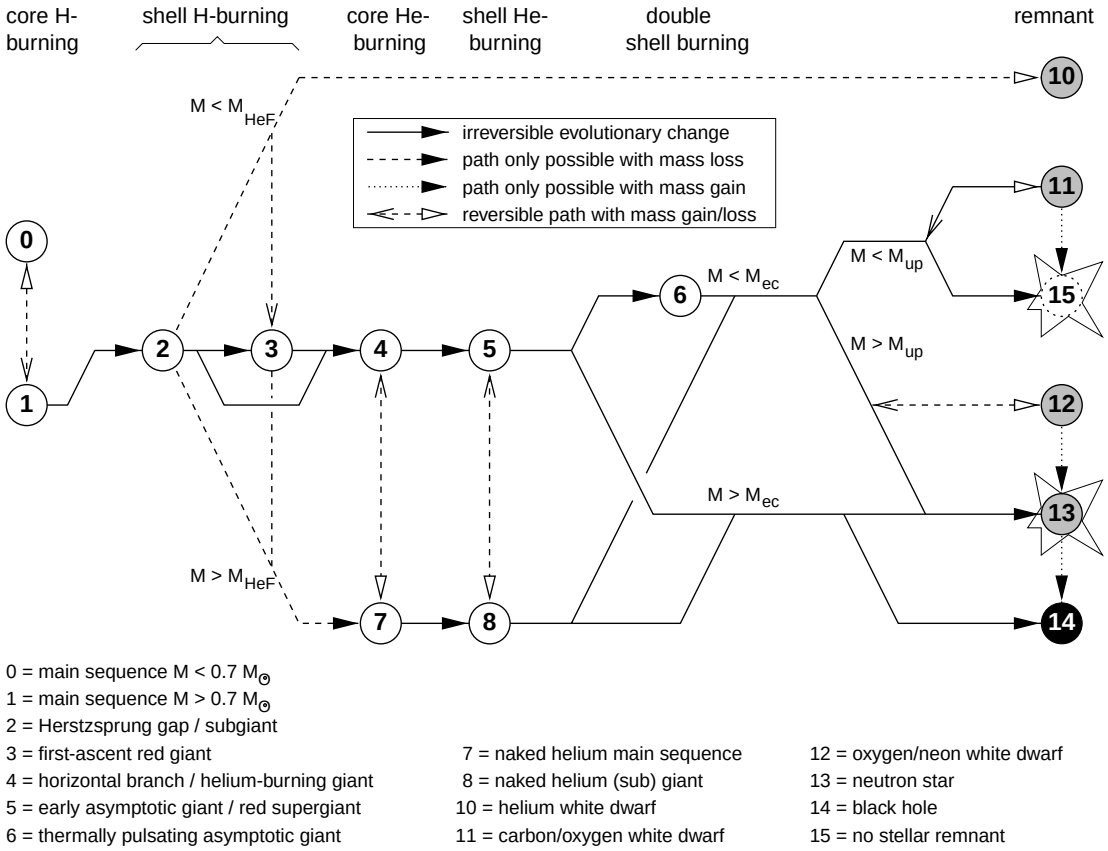

Figure 19. Possible evolution paths through the various stellar evolution phases.

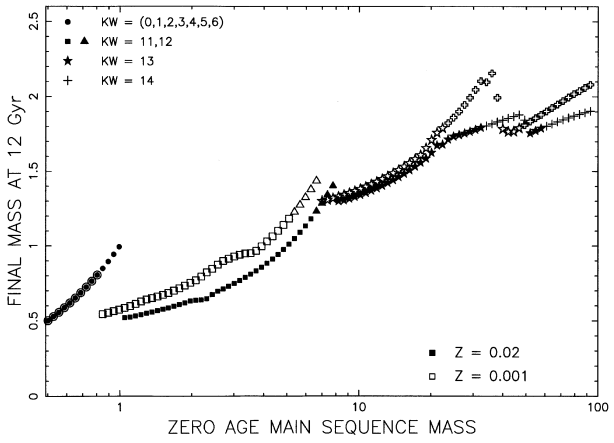

Figure 20. Distribution of remnant masses and types after 1.2×10^{10} yr of evolution, as a function of initial mass, for $Z = 0.001$ (hollow symbols) and $Z = 0.02$ (filled symbols).

In the absence of mass-loss, STAR is required only at the beginning of the evolution, and then HRDIAG can be called at any age to return the correct stellar quantities. When mass-loss is included, HRDIAG must be called often enough that only a small amount of mass is lost during each time-step. STAR also needs to be called often, as some time-scales need to be reset after changes of type, e.g., start of the HeMS, as do some luminosities, e.g., $L_{\rm ZAHB}$ depends on the envelope mass at the helium flash.

The following time-steps, δt_k, are assigned according to the stellar type, k:

$$\delta t_k = \begin{cases} \dfrac{1}{100} t_{\rm MS} & k = 0, 1 \\ \dfrac{1}{20}(t_{\rm BGB} - t_{\rm MS}) & k = 2 \\ \dfrac{1}{50}(t_{\rm inf,1} - t) & k = 3 t \le t_x \\ \dfrac{1}{50}(t_{\rm inf,2} - t) & k = 3 t > t_x \\ \dfrac{1}{50} t_{\rm He} & k = 4 \\ \dfrac{1}{50}(t_{\rm inf,1} - t) & k = 5, 6 t \le t_x \\ \dfrac{1}{50}(t_{\rm inf,2} - t) & k = 5, 6 t > t_x \\ \dfrac{1}{20} t_{\rm HeMS} & k = 7 \\ \dfrac{1}{50}(t_{\rm inf,1} - t) & k = 8, 9 t \le t_x \\ \dfrac{1}{50}(t_{\rm inf,2} - t) & k = 8, 9 t > t_x \\ \max(0.1, 10.0t) & k \ge 10 \end{cases}.$$

In addition, we impose a maximum TPAGB time-step of 5×10^{-3} Myr so that important contributions from the small-envelope pertubation functions are not missed. We also calculate $\delta t_{\rm e}$, the time to the next change of stellar type (e.g., $\delta t_{\rm e} = t_{\rm MS} - t$ for

$k = 0, 1$), and $\delta t_{\rm N}$ which is the current remaining nuclear lifetime of the star (i.e., $\delta t_{\rm N} = t_{\rm N} - t$, assuming that the star is in a nuclear burning stage; otherwise $t_{\rm N}$ is set to some large dummy value). If necessary we limit the time-step such that mass-loss will be less than 1 per cent over the time-step,

$$\delta t_{\rm ml} = -0.01 \frac{M}{\dot{M}},$$

and we also limit the time-step so that the radius will not change by more than 10 per cent,

$$\delta t_R = 0.1 \frac{R}{|\dot{R}|}.$$

Therefore the time-step is given by

$$\delta t = \min(\delta t_{\rm k}, \delta t_{\rm e}, \delta t_{\rm N}, \delta t_{\rm ml}, \delta t_{\rm R}). \quad (112)$$

In some cases the choice of time-steps is purely for aesthetic purposes, so the size could easily be increased with no loss of accuracy if extra speed is required, such as for evolving large stellar populations. For example, the MS can be safely done in one time-step, but then, for an individual star, the hook feature would not appear on a HRD plotted from the resulting output.

Using the SSE package, we can evolve 10 000 stars up to the age of the Galaxy in approximately 100 s of cpu time on a Sun SparcUltra10 workstation (containing a 300-MHz processor). Thus a million stars can be evolved in roughly the time taken to compute one detailed model track. This speed, coupled with the accuracy of the formulae, makes the SSE package ideal for any project that requires information derived from the evolution of a large number of stars. However, the formulae do not render the model grid of Pols et al. (1998) redundant as it contains a wealth of information detailing the interior structure of each star, information that the formulae simply cannot provide. In fact, the two approaches complement one another.

The evolution formulae described in this paper have been incorporated into a rapid binary evolution algorithm so that we can conduct population synthesis involving single stars and binaries. The SSE subroutines have also been added to an *N*-body code for the simulation of cluster populations. In the future we plan to make $\delta_{\rm ov}$ a free parameter as a variable amount of convective overshooting may be preferable, especially in the mass range of 1.0 to 2.0 $M_\odot$. Formulae that describe surface element abundances will also be added so that the rapid evolution code can be used for nucleosynthesis calculations.

To obtain a copy of the SSE package described in this paper, send a request to the authors, who will provide the FORTRAN subroutines by ftp.

ACKNOWLEDGMENTS

JRH thanks Trinity College and the Cambridge Commonwealth Trust for their kind support. CAT is very grateful to PPARC for support from an advanced fellowship. ORP thanks the Institute of Astronomy, Cambridge for supporting a number of visits undertaken during this work. We thank Peter Eggleton for many helpful suggestions, and Sverre Aarseth for useful comments.

REFERENCES

Aarseth S. J., 1996, in Hut P., Makino J., eds, Proc. IAU Symp. 174, Dynamical Evolution of Star Clusters. Kluwer, Dordrecht, p. 161
Baglin A., 1997, 23rd meeting of the IAU, Joint Discussion 14, Kyoto, Japan
Carr B. J., Hawking S. W., 1974, Nat, 248, 30
Carraro G., Girardi L., Bressan A., Chiosi C., 1996, A&A, 305, 849
Charbonnel C., Meynet G., Maeder A., Schaller G., Schaerer D., 1993, A&AS, 101, 415
de Boer K. S., Tucholke H.-J., Schmidt J. H. K., 1997, A&A, 317, L23
Eggleton P. P., 1996, in Hut P., Makino J., eds, Proc. IAU Symp. 174, Dynamical Evolution of Star Clusters. Kluwer, Dordrecht, p. 213
Eggleton P. P., Fitchett M., Tout C. A., 1989, ApJ, 347, 998
Elson R. A. W., Sigurdsson S., Hurley J. R., Davies M. B., Gilmore G. F., 1998, ApJ, 499, L53
Frost C. A., 1997, PhD thesis, Monash Univ.
Hamann W.-R., Koesterke L., 1998, A&A, 335, 1003
Hamann W.-R., Koesterke L., Wessolowski U., 1995, A&A, 299, 151
Hoffleit D., 1983, The Bright Star Catalogue, 4th ed. Yale University Observatory, New Haven
Humphreys R. M., Davidson K., 1994, PASP, 106, 1025
Iben I., Jr, Renzini A., 1983, ARA&A, 21, 271
Jeffery C. S., 1988, MNRAS, 235, 1287
Jeffries R. D., 1997, MNRAS, 288, 585
Kudritzki R. P., Reimers D., 1978, A&A, 70, 227
Kudritzki R. P., Pauldrach A., Puls J., Abbott D. C., 1989, A&A, 219, 205
Lang K. R., 1992, Astrophysical Data. Springer-Verlag
Lattanzio J. C., 1989, ApJ, 344, L25
Mestel L., 1952, MNRAS, 112, 583
Mowlavi N., Schaerer D., Meynet G., Bernasconi P. A., Charbonnel C., Maeder A., 1998, A&AS, 128, 471
Nieuwenhuizen H., de Jager C., 1990, A&A, 231, 134
Noels A., Fraipont-Caro D., Gabriel M., Grevesse N., Demarque P., eds, 1995, Proc. 32nd Liège Int. Astrophys. Colloq., Université de Liège
Nomoto K., 1984, ApJ, 277, 791
Perryman M. A. C., Høg E., Kovalovsky J., Lindegren L., Turon C., 1997, ESA SP-1200
Pols O. R., Tout C. A., Schröder K.-P., Eggleton P. P., Manners J., 1997, MNRAS, 289, 869
Pols O. R., Schröder K. P., Hurley J. R., Tout C. A., Eggleton P. P., 1998, MNRAS, 298, 525
Rappaport S., Verbunt F., Joss P. C., 1983, ApJ, 275, 713
Schaerer D., Meynet G., Maeder A., Schaller G., 1993, A&AS, 98, 523
Schaller G., Schaerer D., Meynet G., Maeder A., 1992, A&AS, 96, 269
Schröder K. P., Pols O. R., Eggleton P. P., 1997, MNRAS, 285, 696
Shapiro S. L., Teukolsky S. A., 1983, Black Holes, White Dwarfs and Neutron Stars. Wiley
Tout C. A., Pols O. R., Eggleton P. P., Han Z., 1996, MNRAS, 281, 257
Tout C. A., Aarseth S. J., Pols O. R., Eggleton P. P., 1997, MNRAS, 291, 732
Van Eck S., Jorissen A., Udry S., Mayor M., Perrier B., 1998, A&A, 329, 971
Vassiliadis E., Wood P. R., 1993, ApJ, 413, 641
Weidemann V., 1987, A&A, 188, 74

APPENDIX A

The *Z*-dependence of the coefficients a_n and b_n is given here. Unless otherwise stated,

$$a_n = \alpha + \beta\zeta + \gamma\zeta^2 + \eta\zeta^3 + \mu\zeta^4,$$

and similarly for b_n, where

$$\zeta = \log(Z/0.02).$$

The variables

$$\sigma = \log(Z)$$

and

$$\rho = \zeta + 1.0$$

are also used.

	α	β	γ	η	μ
a_1	1.593890(+3)	2.053038(+3)	1.231226(+3)	2.327785(+2)	
a_2	2.706708(+3)	1.483131(+3)	5.772723(+2)	7.411230(+1)	
a_3	1.466143(+2)	−1.048442(+2)	−6.795374(+1)	−1.391127(+1)	
a_4	4.141960(−2)	4.564888(−2)	2.958542(−2)	5.571483(−3)	
a_5	3.426349(−1)				
a_6	1.949814(+1)	1.758178(+0)	−6.008212(+0)	−4.470533(+0)	
a_7	4.903830(+0)				
a_8	5.212154(−2)	3.166411(−2)	−2.750074(−3)	−2.271549(−3)	
a_9	1.312179(+0)	−3.294936(−1)	9.231860(−2)	2.610989(−2)	
a_{10}	8.073972(−1)				
a'_{11}	1.031538(+0)	−2.434480(−1)	7.732821(+0)	6.460705(+0)	1.374484(+0)
a'_{12}	1.043715(+0)	−1.577474(+0)	−5.168234(+0)	−5.596506(+0)	−1.299394(+0)
a_{13}	7.859573(+2)	−8.542048(+0)	−2.642511(+1)	−9.585707(+0)	
a_{14}	3.858911(+3)	2.459681(+3)	−7.630093(+1)	−3.486057(+2)	−4.861703(+1)
a_{15}	2.888720(+2)	2.952979(+2)	1.850341(+2)	3.797254(+1)	
a_{16}	7.196580(+0)	5.613746(−1)	3.805871(−1)	8.398728(−2)	

$a_{11} = a'_{11}a_{14}$
$a_{12} = a'_{12}a_{14}$

	α	β	γ	η	μ
a'_{18}	2.187715(−1)	−2.154437(+0)	−3.768678(+0)	−1.975518(+0)	−3.021475(−1)
a'_{19}	1.466440(+0)	1.839725(+0)	6.442199(+0)	4.023635(+0)	6.957529(−1)
a_{20}	2.652091(+1)	8.178458(+1)	1.156058(+2)	7.633811(+1)	1.950698(+1)
a_{21}	1.472103(+0)	−2.947609(+0)	−3.312828(+0)	−9.945065(−1)	
a_{22}	3.071048(+0)	−5.679941(+0)	−9.745523(+0)	−3.594543(+0)	
a_{23}	2.617890(+0)	1.019135(+0)	−3.292551(−2)	−7.445123(−2)	
a_{24}	1.075567(−2)	1.773287(−2)	9.610479(−3)	1.732469(−3)	
a_{25}	1.476246(+0)	1.899331(+0)	1.195010(+0)	3.035051(−1)	
a_{26}	5.502535(+0)	−6.601663(−2)	9.968707(−2)	3.599801(−2)	

$\log a_{17} = \max[0.097 - 0.1072(\sigma + 3), \max\{0.097, \min[0.1461, 0.1461 + 0.1237(\sigma + 2)]\}]$
$a_{18} = a'_{18}a_{20}$
$a_{19} = a'_{19}a_{20}$

	α	β	γ	η
a_{27}	9.511033(+1)	6.819618(+1)	−1.045625(+1)	−1.474939(+1)
a_{28}	3.113458(+1)	1.012033(+1)	−4.650511(+0)	−2.463185(+0)
a'_{29}	1.413057(+0)	4.578814(−1)	−6.850581(−2)	−5.588658(−2)
a_{30}	3.910862(+1)	5.196646(+1)	2.264970(+1)	2.873680(+0)
a_{31}	4.597479(+0)	−2.855179(−1)	2.709724(−1)	
a_{32}	6.682518(+0)	2.827718(−1)	−7.294429(−2)	

$a_{29} = a'^{a_{32}}_{29}$

	α	β	γ	η
a_{34}	1.910302(−1)	1.158624(−1)	3.348990(−2)	2.599706(−3)
a_{35}	3.931056(−1)	7.277637(−2)	−1.366593(−1)	−4.508946(−2)
a_{36}	3.267776(−1)	1.204424(−1)	9.988332(−2)	2.455361(−2)
a_{37}	5.990212(−1)	5.570264(−2)	6.207626(−2)	1.777283(−2)

$a_{33} = \min(1.4, 1.5135 + 0.3769\zeta)$
$a_{33} = \max[0.6355 - 0.4192\zeta, \max(1.25, a_{33})]$

	α	β	γ	η
a_{38}	7.330122(−1)	5.192827(−1)	2.316416(−1)	8.346941(−3)
a_{39}	1.172768(+0)	−1.209262(−1)	−1.193023(−1)	−2.859837(−2)
a_{40}	3.982622(−1)	−2.296279(−1)	−2.262539(−1)	−5.219837(−2)
a_{41}	3.571038(+0)	−2.223625(−2)	−2.611794(−2)	−6.359648(−3)
a_{42}	1.9848(+0)	1.1386(+0)	3.5640(−1)	
a_{43}	6.300(−2)	4.810(−2)	9.840(−3)	
a_{44}	1.200(+0)	2.450(+0)		

$a_{42} = \min[1.25, \max(1.1, a_{42})]$
$a_{44} = \min[1.3, \max(0.45, a_{44})]$

	α	β	γ	η
a_{45}	2.321400(−1)	1.828075(−3)	−2.232007(−2)	−3.378734(−3)
a_{46}	1.163659(−2)	3.427682(−3)	1.421393(−3)	−3.710666(−3)
a_{47}	1.048020(−2)	−1.231921(−2)	−1.686860(−2)	−4.234354(−3)
a_{48}	1.555590(+0)	−3.223927(−1)	−5.197429(−1)	−1.066441(−1)
a_{49}	9.7700(−2)	−2.3100(−1)	−7.5300(−2)	
a_{50}	2.4000(−1)	1.8000(−1)	5.9500(−1)	
a_{51}	3.3000(−1)	1.3200(−1)	2.1800(−1)	
a_{52}	1.1064(+0)	4.1500(−1)	1.8000(−1)	
a_{53}	1.1900(+0)	3.7700(−1)	1.7600(−1)	

$a_{49} = \max(a_{49}, 0.145)$
$a_{50} = \min(a_{50}, 0.306 + 0.053\zeta)$
$a_{51} = \min(a_{51}, 0.3625 + 0.062\zeta)$
$a_{52} = \max(a_{52}, 0.9)$
$a_{52} = \min(a_{52}, 1.0) \quad \text{for } Z > 0.01$
$a_{53} = \max(a_{53}, 1.0)$
$a_{53} = \min(a_{53}, 1.1) \quad \text{for } Z > 0.01$

	α	β	γ	η	μ
a_{54}	3.855707(−1)	−6.104166(−1)	5.676742(+0)	1.060894(+1)	5.284014(+0)
a_{55}	3.579064(−1)	−6.442936(−1)	5.494644(+0)	1.054952(+1)	5.280991(+0)
a_{56}	9.587587(−1)	8.777464(−1)	2.017321(−1)		

$a_{57} = \min(1.4, 1.5135 + 0.3769\zeta)$
$a_{57} = \max[0.6355 - 0.4192\zeta, \ \max(1.25, a_{57})]$

	α	β	γ	η	μ
a_{58}	4.907546(−1)	−1.683928(−1)	−3.108742(−1)	−7.202918(−2)	
a_{59}	4.537070(+0)	−4.465455(+0)	−1.612690(+0)	−1.623246(+0)	
a_{60}	1.796220(+0)	2.814020(−1)	1.423325(+0)	3.421036(−1)	
a_{61}	2.256216(+0)	3.773400(−1)	1.537867(+0)	4.396373(−1)	
a_{62}	8.4300(−2)	−4.7500(−2)	−3.5200(−2)		
a_{63}	7.3600(−2)	7.4900(−2)	4.4260(−2)		
a_{64}	1.3600(−1)	3.5200(−2)			
a_{65}	1.564231(−3)	1.653042(−3)	−4.439786(−3)	−4.951011(−3)	−1.216530(−3)
a_{66}	1.4770(+0)	2.9600(−1)			
a_{67}	5.210157(+0)	−4.143695(+0)	−2.120870(+0)		
a_{68}	1.1160(+0)	1.6600(−1)			

$a_{62} = \max(0.065, a_{62})$
$a_{63} = \min(0.055, a_{63}) \quad \text{for } Z < 0.004$
$a_{64} = \max[0.091, \ \min(0.121, a_{64})]$
$a_{66} = \max[a_{66}, \ \min(1.6, -0.308 - 1.046\zeta)]$
$a_{66} = \max[0.8, \ \min(0.8 - 2.0\zeta, a_{66})]$
$a_{68} = \max[0.9, \ \min(a_{68}, 1.0)]$
$a_{64} = B = \alpha_R(M = a_{66}) \quad \text{for } a_{68} > a_{66}$
$a_{68} = \min(a_{68}, a_{66})$

	α	β	γ	η
a_{69}	1.071489(+0)	−1.164852(−1)	−8.623831(−2)	−1.582349(−2)
a_{70}	7.108492(−1)	7.935927(−1)	3.926983(−1)	3.622146(−2)
a_{71}	3.478514(+0)	−2.585474(−2)	−1.512955(−2)	−2.833691(−3)
a_{72}	9.132108(−1)	−1.653695(−1)		3.636784(−2)
a_{73}	3.969331(−3)	4.539076(−3)	1.720906(−3)	1.897857(−4)
a_{74}	1.600(+0)	7.640(−1)	3.322(−1)	

$a_{72} = \max(a_{72}, 0.95) \quad \text{for } Z > 0.01$
$a_{74} = \max[1.4, \ \min(a_{74}, 1.6)]$

	α	β	γ	η
a_{75}	8.109(−1)	−6.282(−1)		
a_{76}	1.192334(−2)	1.083057(−2)	1.230969(+0)	1.551656(+0)
a_{77}	−1.668868(−1)	5.818123(−1)	−1.105027(+1)	−1.668070(+1)
a_{78}	7.615495(−1)	1.068243(−1)	−2.011333(−1)	−9.371415(−2)
a_{79}	9.409838(+0)	1.522928(+0)		
a_{80}	−2.7110(−1)	−5.7560(−1)	−8.3800(−2)	
a_{81}	2.4930(+0)	1.1475(+0)		

$a_{75} = \max[1.0,\ \min(a_{75}, 1.27)]$
$a_{75} = \max(a_{75}, 0.6355 - 0.4192\zeta)$
$a_{76} = \max(a_{76}, -0.1015564 - 0.2161264\zeta - 0.05182516\zeta^2)$
$a_{77} = \max[-0.3868776 - 0.5457078\zeta - 0.1463472\zeta^2,\ \min(0.0, a_{77})]$
$a_{78} = \max[0.0,\ \min(a_{78}, 7.454 + 9.046\zeta)]$
$a_{79} = \min[a_{79},\ \max(2.0, -13.3 - 18.6\zeta)]$
$a_{80} = \max(0.0585542, a_{80})$
$a_{81} = \min[1.5,\ \max(0.4, a_{81})]$

	α	β	γ	η	μ
b_1	3.9700(−1)	2.8826(−1)	5.2930(−1)		
b_4	9.960283(−1)	8.164393(−1)	2.383830(+0)	2.223436(+0)	8.638115(−1)
b_5	2.561062(−1)	7.072646(−2)	−5.444596(−2)	−5.798167(−2)	−1.349129(−2)
b_6	1.157338(+0)	1.467883(+0)	4.299661(+0)	3.130500(+0)	6.992080(−1)
b_7	4.022765(−1)	3.050010(−1)	9.962137(−1)	7.914079(−1)	1.728098(−1)

$b_1 = \min(0.54, b_1)$
$b_2 = 10^{-4.6739-0.9394\sigma}$
$b_2 = \min[\max(b_2, -0.04167 + 55.67Z), 0.4771 - 9329.21Z^{2.94}]$
$b'_3 = \max(-0.1451, -2.2794 - 1.5175\sigma - 0.254\sigma^2)$
$b_3 = 10^{b'_3}$
$b_3 = \max(b_3, 0.7307 + 14265.1Z^{3.395})$ for $Z > 0.004$
$b_4 = b_4 + 0.1231572\zeta^5$
$b_6 = b_6 + 0.01640687\zeta^5$

	α	β	γ
b_9	2.751631(+3)	3.557098(+2)	
b_{10}	−3.820831(−2)	5.872664(−2)	
b'_{11}	1.071738(+2)	−8.970339(+1)	−3.949739(+1)
b_{12}	7.348793(+2)	−1.531020(+2)	−3.793700(+1)
b'_{13}	9.219293(+0)	−2.005865(+0)	−5.561309(−1)

$b_{11} = b'^2_{11}$
$b_{13} = b'^2_{13}$

	α	β	γ
b'_{14}	2.917412(+0)	1.575290(+0)	5.751814(−1)
b_{15}	3.629118(+0)	−9.112722(−1)	1.042291(+0)
b'_{16}	4.916389(+0)	2.862149(+0)	7.844850(−1)

$b_{14} = b'^{b_{15}}_{14}$
$b_{16} = b'^{b_{15}}_{16}$
$b_{17} = 1.0$
$b_{17} = 1.0 - 0.3880523(\zeta + 1.0)^{2.862149}$ for $\zeta > -1.0$

	α	β	γ	η
b_{18}	5.496045(+1)	−1.289968(+1)	6.385758(+0)	
b_{19}	1.832694(+0)	−5.766608(−2)	5.696128(−2)	
b_{20}	1.211104(+2)			
b_{21}	2.214088(+2)	2.187113(+2)	1.170177(+1)	−2.635340(+1)
b_{22}	2.063983(+0)	7.363827(−1)	2.654323(−1)	−6.140719(−2)
b_{23}	2.003160(+0)	9.388871(−1)	9.656450(−1)	2.362266(−1)
b'_{24}	1.609901(+1)	7.391573(+0)	2.277010(+1)	8.334227(+0)
b_{25}	1.747500(−1)	6.271202(−2)	−2.324229(−2)	−1.844559(−2)
b'_{27}	2.752869(+0)	2.729201(−2)	4.996927(−1)	2.496551(−1)
b_{28}	3.518506(+0)	1.112440(+0)	−4.556216(−1)	−2.179426(−1)

$b_{24} = b'^{b_{28}}_{24}$
$b_{26} = 5.0 - 0.09138012Z^{-0.3671407}$
$b_{27} = b'^{2b_{28}}_{27}$

	α	β	γ	η
b_{29}	1.626062(+2)	−1.168838(+1)	−5.498343(+0)	
b_{30}	3.336833(−1)	−1.458043(−1)	−2.011751(−2)	
b'_{31}	7.425137(+1)	1.790236(+1)	3.033910(+1)	1.018259(+1)
b_{32}	9.268325(+2)	−9.739859(+1)	−7.702152(+1)	−3.158268(+1)
b_{33}	2.474401(+0)	3.892972(−1)		
b'_{34}	1.127018(+1)	1.622158(+0)	−1.443664(+0)	−9.474699(−1)

$b_{31} = b'^{b_{33}}_{31}$
$b_{34} = b'^{b_{33}}_{34}$

	α	β	γ	η
b'_{36}	1.445216(−1)	−6.180219(−2)	3.093878(−2)	1.567090(−2)
b'_{37}	1.304129(+0)	1.395919(−1)	4.142455(−3)	−9.732503(−3)
b'_{38}	5.114149(−1)	−1.160850(−2)		

$b_{36} = b'^4_{36}$
$b_{37} = 4.0b'_{37}$
$b_{38} = b'^4_{38}$

	α	β	γ	η
b_{39}	1.314955(+2)	2.009258(+1)	−5.143082(−1)	−1.379140(+0)
b_{40}	1.823973(+1)	−3.074559(+0)	−4.307878(+0)	
b'_{41}	2.327037(+0)	2.403445(+0)	1.208407(+0)	2.087263(−1)
b_{42}	1.997378(+0)	−8.126205(−1)		
b_{43}	1.079113(−1)	1.762409(−2)	1.096601(−2)	3.058818(−3)
b'_{44}	2.327409(+0)	6.901582(−1)	−2.158431(−1)	−1.084117(−1)

$b_{40} = \max(b_{40}, 1.0)$
$b_{41} = b'^{b_{42}}_{41}$
$b_{44} = b'^5_{44}$

	α	β	γ	η
b_{46}	2.214315(+0)	−1.975747(+0)		
b_{48}	5.072525(+0)	1.146189(+1)	6.961724(+0)	1.316965(+0)
b_{49}	5.139740(+0)			

$b_{45} = 1.0 - (2.47162\rho - 5.401682\rho^2 + 3.247361\rho^3)$
$b_{45} = 1.0 \quad \text{for } \rho \leq 0.0$
$b_{46} = -1.0b_{46}\log\left(\frac{M_{\rm HeF}}{M_{\rm FGB}}\right)$
$b_{47} = 1.127733\rho + 0.2344416\rho^2 - 0.3793726\rho^3$

	α	β	γ	η	μ
b'_{51}	1.125124(+0)	1.306486(+0)	3.622359(+0)	2.601976(+0)	3.031270(−1)
b_{52}	3.349489(−1)	4.531269(−3)	1.131793(−1)	2.300156(−1)	7.632745(−2)
b'_{53}	1.467794(+0)	2.798142(+0)	9.455580(+0)	8.963904(+0)	3.339719(+0)
b_{54}	4.658512(−1)	2.597451(−1)	9.048179(−1)	7.394505(−1)	1.607092(−1)
b_{55}	1.0422(+0)	1.3156(−1)	4.5000(−2)		
b'_{56}	1.110866(+0)	9.623856(−1)	2.735487(+0)	2.445602(+0)	8.826352(−1)
b'_{57}	−1.584333(−1)	−1.728865(−1)	−4.461431(−1)	−3.925259(−1)	−1.276203(−1)

$b_{51} = b'_{51} - 0.1343798\zeta^5$
$b_{53} = b'_{53} + 0.4426929\zeta^5$
$b_{55} = \min(0.99164 - 743.123Z^{2.83}, b_{55})$
$b_{56} = b'_{56} + 0.1140142\zeta^5$
$b_{57} = b'_{57} - 0.01308728\zeta^5$
Note that $x(n)$ for some number x represents $x \times 10^n$.
A blank entry in a table implies a zero value.

This paper has been typeset from a TEX/LATEX file prepared by the author.